Inorganic Chemistry

Article

pubs.acs.org/IC

Interplay of Metallophilic Interactions, $\pi-\pi$ Stacking, and Ligand Substituent Effects in the Structures and Luminescence Properties of Neutral Pt^{II} and Pd^{II} Aryl Isocyanide Complexes

Ilya M. Sluch,[†] Anthea J. Miranda,[†] Oussama Elbjeirami,[‡,§] Mohammad A. Omary,[‡] and LeGrande M. Slaughter*[,†]

[†]Department of Chemistry, Oklahoma State University, Stillwater, Oklahoma 74078, United States

[‡]Department of Chemistry, University of North Texas, Denton, Texas 76203, United States

Supporting Information

ABSTRACT: Packing interactions in the crystal structures of a series of *cis*-$M(CNAr)_2Cl_2$ complexes (M = Pt, Pd; Ar = substituted phenyl) were examined and correlated with the luminescence properties of the Pt complexes. The structures of the PhNC and *p*-tolyl isocyanide complexes exhibit extended chains of metallophilic interactions with M···M distances of 3.24−3.25 and 3.34 Å, respectively, with nearly isostructural Pt and Pd compounds. Both structure types contain void channels running parallel to the M···M chains. The channels are 3−4 Å wide and vacant for the phenyl structures, while those in the *p*-tolyl structures are up to 7.6 Å wide and contain water. These channeled structures are stabilized by a combination of metallophilic bonding and aryl $\pi-\pi$ stacking interactions. The Pt structure with 4-F substituents also features extended Pt···Pt chains, but with longer 3.79 Å distances alternating with shorter 3.37 Å contacts. Structures with 4-CF_3 and 4-OMe substituents exhibit mostly isolated dimers of M···M contacts. In complexes with 2,6-dimethylphenyl isocyanide, steric hindrance precludes any short M···M contacts. The primary effect of aryl substitution is to provide alternative packing motifs, such as $CF_3\cdots\pi$ and $CH_3\cdots\pi$ interactions, that either augment or disrupt the combination of metallophilic contacts and $\pi-\pi$ stacking needed to stabilize extended M···M chains. Differences in the Pt and Pd structures containing 4-F and 4-OMe substituents are consistent with a higher driving force for metallophilic interactions for Pt versus Pd. The M−C and M−Cl bond distances indicate a slightly higher trans influence for aryl isocyanides bound to Pt versus Pd. The three extended Pt···Pt chain structures display luminescence assignable to ($d\sigma^*\rightarrow p\sigma$) excited states, demonstrating the existence of substantial orbital communication along the metal−metal chains. Face-indexing shows that the preferred crystal growth axis is along the metal−metal chains for the luminescent structures. Variable temperature structural studies showed that both M···M and $\pi-\pi$ interactions contract upon cooling. Overall, this study suggests that synergy with $\pi-\pi$ and other interactions is necessary to stabilize extended M···M chain structures. Thus, efforts to design functional materials based on metallophilic bonding must consider the full array of available packing motifs.

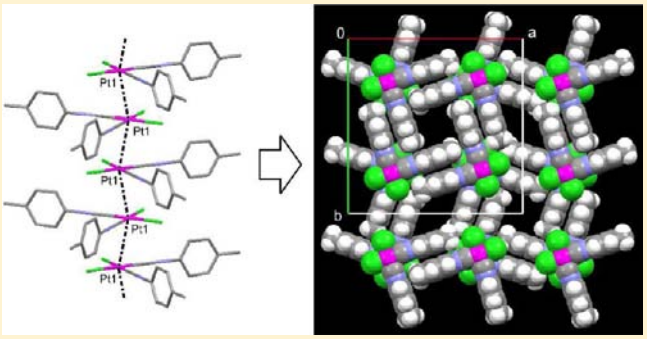

INTRODUCTION

Attractive "metallophilic" interactions between d^8, d^{10}, and s^2 metal ions are increasingly being recognized as important determinants of solid-state structure as well as potential sources of useful material properties.[1] These attractions, which are attributed to correlation effects enhanced by relativistic effects,[2] can manifest themselves in the crystalline state as dimers, oligomers, extended chains, or sheets of metal complexes with M···M contacts less than the sum of van der Waals radii.[3] The electronic communication facilitated by these interactions can lead to a number of interesting properties. Partial oxidation of $[Pt(CN)_4]^{2-}$ salts results in contraction of the Pt···Pt distances from 3.3 Å to 2.7−3.0 Å with concomitant onset of one-dimensional electrical conductivity.[4] These same salts also display strong luminescence that depends on the presence of short M···M contacts,[5] as do a range of square planar Pt^{II} and linear Ag^I and Au^I complexes.[1b,6] Pt^{II} diimine complexes crystallize as different polymorphs that have distinct colors as a result of changes in crystal packing or solvation effects that modulate the Pt···Pt distances.[7] Metallophilic attractions are much weaker than covalent bonds but can be as strong as hydrogen bonds.[2] This relative weakness means that these interactions can be easily disrupted by steric effects as well as by other crystal packing forces such as $\pi-\pi$,[8] CH−π,[9] metal−π,[10] hydrogen bonding,[11] and halogen bonding[12] interactions. However, metallophilic bonding often coexists with these other packing motifs,[13] suggesting that a suitable combination

Received: May 25, 2012
Published: October 1, 2012

   dx.doi.org/10.1021/ic301104a | Inorg. Chem. 2012, 51, 10728−10746

of packing forces can synergistically stabilize the M···M interactions. This interplay of packing interactions is likely responsible for the known tendency of some metal complexes to form polymorphs that differ in the degree of metal−metal contact and exhibit distinct properties.[7,14] Particularly intriguing are examples in which the extent of metal−metal interaction changes upon incorporation of solvents into the crystalline lattice.[7,15] Such complexes can display so-called vapochromic[15e,h−j,n,16] and/or vapoluminescent[13m,15d,f,g,o−r,17] behavior, in which diffusion of volatile organic compounds into voids or channels in the crystal structure induces changes in color or luminescence properties, respectively. Because these phenomena are potentially useful in the design of sensors,[15o,18] understanding the factors that favor channeled or porous structures containing metallophilic interactions is an important goal.

We recently reported new polymorphs of $M(CNPh)_2Cl_2$ (M = Pt, Pd) that represent the first examples of extended M···M chain compounds containing solvent-free channels.[19] The channels appear to be stabilized by a synergistic combination of metallophilic and aryl $\pi-\pi$ interactions. The chain form of $Pt(CNPh)_2Cl_2$ is luminescent under UV excitation, whereas the previously known dimeric form[20] is nonluminescent, clearly indicating that luminescence in the compound requires extended Pt···Pt contacts. However, the channels are too narrow (3.0−4.0 Å) to admit solvents that might perturb the Pt···Pt bonding and thus the luminescence properties. Toward an eventual goal of designing luminescent materials with tunable pore sizes for sensing of volatile molecules, we have studied the structures and luminescence properties of a series of Pt and Pd dichloride complexes of substituted arylisocyanide ligands (Chart 1). Isocyanide ligands are both strong σ-donors

Chart 1. Isocyanide Complexes Studied in This Work

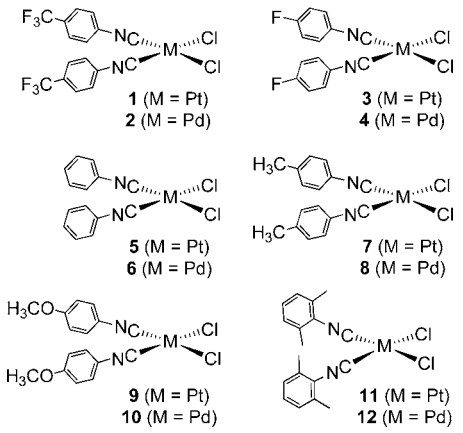

and appreciable π-acceptors; both properties are thought to reinforce M···M interactions.[21] Extended metallophilic bonding has been reported in isocyanide-containing double salts of the type $[Pt(CNR)_4][PtX_4]$ (X = anionic donor)[15e,22] as well as in neutral complexes of the types $Pt(CNR)_2(CN)_2$[15f,23] and (benzoquinolinate)Pt(CNR)Cl.[13j] However, the structures and luminescence properties of neutral Pt^{II} bis(isocyanide) dihalide complexes have not been systematically studied, despite the fact that analogous linear halide−isocyanide complexes of Au^I are known to be strongly luminescent and to engage in extensive metallophilic bonding.[21a,c,d,24]

This study aims to examine the electronic effects on metallophilic bonding of placing different electron-withdrawing and -donating groups on the arylisocyanide ligands while also exploring the steric effects of this substitution. A simple orbital depiction predicts that metallophilic attractions should be enhanced by configuration interaction of the filled bands arising from metal d_{z^2} orbitals with empty p and s bands, resulting in a net stabilization of the d_{z^2} electrons.[7] We hypothesize that adding electron-donor substituents should strengthen metallophilic bonding by raising the antibonding d_{z^2} ($d\sigma^*$) states in energy, thereby increasing the degree of configuration interaction. However, these substituents also change the steric profile of the arylisocyanide, which may either disrupt or enhance the $\pi-\pi$ stacking interactions that can synergistically stabilize extended M···M interactions in these complexes.[19] Another goal of this study is to compare the structures of identically ligated palladium and platinum complexes in order to gain insights into the relative importance of metallophilic attractions versus other packing forces. Owing to the lanthanide contraction, Pt has a very similar covalent radius to Pd[25,26] and often forms nearly isostructural complexes,[27] but Pd experiences smaller relativistic effects that are believed to impart weaker metallophilic bonding.[2a,28] Therefore, any significant differences in the crystal structures of isoleptic Pd and Pt complexes may indicate that metallophilic interactions play a key structure-directing role. We also report spectroscopic studies confirming that luminescence depends on the presence of extended Pt···Pt chains and temperature-dependent crystallographic studies that identify which intermolecular interactions dominate at lower temperatures as thermal motion is attenuated. All of these studies suggest that stabilization of luminescent structures containing Pt···Pt chains requires a synergistic combination of metallophilic bonding with $\pi-\pi$, and sometimes CH···π, interactions. Importantly, these synergistic packing arrangements can stabilize luminescent structures containing extended channels. In the case of $Pt/Pd(CNC_6H_4$-p-$CH_3)_2Cl_2$, we have identified channels with the largest continuous widths yet reported for structures containing metallophilic interactions.

EXPERIMENTAL SECTION

General Considerations. All manipulations were performed under air at ambient temperature. CH_2Cl_2 (Pharmco) was washed with concentrated H_2SO_4, water, aqueous $NaHCO_3$, and again water, and then distilled from P_2O_5 prior to use. Hexanes (Pharmco), *n*-hexane (Acros, 95%), cyclohexane (Acros, p.a.), and Et_2O (Acros) were dried over and distilled from Na/benzophenone ketyl prior to use. Chlorobenzene (Aldrich, 99+% spectrophotometric grade) and 1,2-dichlorobenzene (Acros, 99%) were used as received. NMR solvents were purchased from Cambridge Isotope Laboratories. CD_3CN and $CDCl_3$ were used as received. CD_2Cl_2 was dried by stirring over activated 4 Å molecular sieves, and then stored over and vacuum distilled from P_2O_5 prior to use. 2,6-Dimethylphenyl isocyanide (≥98%) was purchased from Fluka and used as received. All other arylisocyanides were synthesized from the corresponding anilines via phase-transfer Hofmann reactions.[29] ***Caution!*** *Aryl isocyanides are vile-smelling liquids that must be handled in well-ventilated fume hoods.* (COD)$PdCl_2$ and (COD)$PtCl_2$ were prepared by literature procedures.[30]

NMR spectra were recorded on Varian GEMINI 2000 (300 MHz) and Unity INOVA (400 and 600 MHz) spectrometers. IR spectra were acquired on a Perkin-Elmer System 2000 FT-IR or a Thermo Nexus 670 FT-IR with 0.5 cm^{-1} resolution and weak apodization. Elemental analyses were performed by Desert Analytics (Tucson, Arizona) or Midwest Microlab (Indianapolis, Indiana).

Synthesis of Isocyanide Complexes. A modification of a published route to similar complexes[31] was used. Isocyanide (2.2

dx.doi.org/10.1021/ic301104a | *Inorg. Chem.* 2012, 51, 10728−10746

Table 1. Crystallographic Data for Complexes 1−8

	1	2	3	3	4
formula	$C_{16}H_8Cl_2F_6N_2Pt$	$C_{16}H_8Cl_2F_6N_2Pd$	$C_{14}H_8Cl_2F_2N_2Pt$	$C_{14}H_8Cl_2F_2N_2Pt$	$C_{14}H_8Cl_2F_2N_2Pd$
M_r	608.23	519.54	508.21	508.21	419.52
T (K)	115(2)	100(2)	115(2)	300(2)	115(2)
cryst syst	monoclinic	monoclinic	monoclinic	monoclinic	triclinic
space group	$P2_1/c$	$P2_1/c$	$P2_1/n$	$P2_1/n$	$P\bar{1}$
a (Å)	14.2940(9)	14.7788(10)	6.7933(2)	6.9450(2)	9.5569(4)
b (Å)	17.9417(11)	17.9280(11)	18.2047(5)	18.2518(7)	13.2609(5)
c (Å)	14.7000(9)	14.0492(10)	24.2898(6)	24.5576(9)	24.577(1)
α (deg)	90	90	90	90	97.089(3)
β (deg)	93.597(4)	91.740(4)	90.084(2)	90.897(2)	94.043(2)
γ (deg)	90	90	90	90	104.483(2)
V (Å^3)	3762.5(4)	3720.7(4)	3003.92(14)	3112.5(2)	2976.0(2)
Z	8	8	8	8	8
D_{calcd} (g cm^{-3})	2.147	1.855	2.247	2.169	1.873
μ (mm^{-1})	7.802	1.345	9.711	9.711	1.619
reflns measured	43 604	41 955	63 428	36 446	36 222
reflns unique [R_{int}]	9320 [0.0323]	10 152 [0.0390]	7427 [0.0563]	7729 [0.0339]	16 700 [0.0509]
reflns obsd [$I > 2\sigma(I)$]	8130	8231	7156	5744	14 880
R1, wR2 [$I > 2\sigma(I)$]	0.0218, 0.0496	0.0301, 0.0629	0.0278, 0.0722	0.0296, 0.0527	0.0484, 0.1261
R1, wR2 (all data)	0.0288, 0.0527	0.0430, 0.0679	0.0291, 0.0727	0.0505, 0.0585	0.0566, 0.1298

	5a[a]	6a[a]	7	8
formula	$C_{14}H_{10}Cl_2N_2Pt$	$C_{14}H_{10}Cl_2N_2Pd$	$C_{16}H_{14}Cl_2N_2Pt$	$C_{16}H_{14}Cl_2N_2Pd$
M_r	472.23	383.54	500.28[b]	411.59[b]
T (K)	300(2)	300(2)	298(2)	298(2)
cryst syst	monoclinic	monoclinic	tetragonal	tetragonal
space group	$P2_1/c$	$P2_1/c$	$P4/mnc$	$P4/mnc$
a (Å)	15.9578(6)	15.9320(3)	24.5366(1)	24.5268(2)
b (Å)	15.3189(5)	15.3613(4)	24.5366(1)	24.5268(2)
c (Å)	6.5520(3)	6.5166(1)	6.5728(1)	6.5445(1)
α (deg)	90	90	90	90
β (deg)	92.184(2)	92.144(1)	90	90
γ (deg)	90	90	90	90
V (Å^3)	1600.51(11)	1593.73(6)	3957.12(6)	3936.94(8)
Z	4	4	8	8
$D_{calcd.}$ (g cm^{-3})	1.960	1.598	1.679[b]	1.389[b]
μ (mm^{-1})	9.088	1.486	7.356	1.209
reflns measured	34 875	38 374	31 545	21 135
reflns unique [R_{int}]	6574 [0.0439]	7208 [0.0408]	2043 [0.0315]	2661 [0.0309]
reflns obsd [$I > 2\sigma(I)$]	5540	5460	1706	2109
R1, wR2 [$I > 2\sigma(I)$]	0.0391, 0.1138	0.0262, 0.0589	0.0188, 0.0453	0.0397, 0.0979
R1, wR2 (all data)	0.0482, 0.1189	0.0415, 0.0637	0.0260, 0.0470	0.0515, 0.1024

[a]Structural data for **5a**,**b** and **6a** at 100 K and **6b** at 115 K were previously communicated (ref 19). [b]Calculated from data treated with SQUEEZE.

equiv) was added to a stirred solution of $(COD)MCl_2$ (0.20−0.65 mmol) in 10 mL of dry CH_2Cl_2, and the mixture was stirred for 10 min at 25 °C. Dropwise addition of dry hexanes and dry Et_2O resulted in precipitation of a yellow crystalline solid, which was filtered, washed with dry hexanes and dry Et_2O, and dried in vacuo overnight. Characterization data for $Pd(CNC_6H_4\text{-}p\text{-}CF_3)_2Cl_2$ (**2**),[32] $Pt(CNPh)_2Cl_2$ (**5**),[19] and $Pd(CNPh)_2Cl_2$ (**6**)[19] were previously reported. Data for newly characterized compounds are given below.

*$Pt(CNC_6H_4\text{-}p\text{-}CF_3)_2Cl_2$ (**1**).* Yield 0.206 g, 93%. ^{1}H NMR (300 MHz, $CDCl_3$): δ 7.76 (8H, AB, J = 9.0 Hz, C = 6.0 Hz). ^{13}C NMR (151 MHz, CD_3CN): δ 133.0 (q, $^2J_{CF}$ =33 Hz, Ar *para*), 130.0 (m, ArNC), 129.1 (s, Ar *ortho*), 128.0 (q, $^3J_{CF}$ =3.8 Hz, Ar *meta*), 124.4 (q, $^1J_{CF}$ = 272 Hz, CF_3), 116.0 (br s, Ar *ipso*). IR (Nujol mull): ν_{max}/cm^{-1} 2242 (m), 2207 (m). Anal. Calcd for $C_{16}H_8N_2F_6Cl_2Pt$: C, 31.59, H, 1.33, N, 4.61. Found: C, 31.63, H, 1.47, N, 4.61%.

*$Pt(CNC_6H_4\text{-}p\text{-}F)_2Cl_2$ (**3**).* Yield 0.148 g, 72%. ^{1}H NMR (400 MHz, CD_3CN): 7.70 (4H, m, *ortho* H), 7.28 (4H, m, *meta* H). ^{13}C NMR (151 MHz, CD_2Cl_2): δ 163.9 (d, $^1J_{CF}$ = 254 Hz, Ar *para*), 129.9 (d, $^3J_{CF}$ = 9.5 Hz, Ar *ortho*), 122.5 (s, ArNC), 117.6 (d, $^2J_{CF}$ = 24 Hz, Ar *meta*), 113.9 (m, Ar *ipso*). IR (Nujol mull) ν_{max}/cm^{-1}: 2255 (m), 2218 (m), 2202 (w). Anal. Calcd for $C_{14}H_8N_2F_2Cl_2Pt$: C, 33.09, H, 1.59, N, 5.51. Found: C, 33.06, H, 1.65, N, 5.51.

*$Pd(CNC_6H_4\text{-}p\text{-}F)_2Cl_2$ (**4**).* Yield 0.216 g, 79%. ^{1}H NMR (400 MHz, CD_3CN): 7.71 (4H, m, *ortho* H), 7.30 (4H, m, *meta* H). ^{13}C NMR (151 MHz, CD_2Cl_2): δ 164.3 (d, $^1J_{CF}$ = 255 Hz, Ar *para*), 130.0 (d, $^3J_{CF}$ = 9.5 Hz, Ar *ortho*), 125.1 (br s, ArNC), 122.0 (br s, Ar *ipso*), 117.9 (d, $^2J_{CF}$ = 24 Hz, Ar *meta*). IR (Nujol mull) ν_{max}/cm^{-1}: 2244 (m), 2241 (m), 2227 (m). Anal. Calcd for $C_{14}H_8N_2F_2Cl_2Pd$: C, 40.08, H, 1.92, N, 6.68. Found: C, 40.26, H, 2.14, N, 6.60.

*$Pt(CNC_6H_4\text{-}p\text{-}CH_3)_2Cl_2$ (**7**).* Yield 0.151 g, 82%. ^{1}H NMR (400 MHz, CD_3CN): δ 7.43 (8H, AB, J = 8.9 Hz, C = 32 Hz), 2.40 (6H, s, CH_3). ^{13}C NMR (151 MHz, CD_3CN): δ 143.3 (s, Ar *para*), 131.3 (s, Ar *ortho*), 127.8 (s, Ar *meta*), 124.1 (br s, ArNC), 112.8 (br s, Ar *ipso*), 21.5 (CH_3). IR (Nujol mull) ν_{max}/cm^{-1} 2255 (m), 2216 (m). Anal. Calcd for $C_{16}H_{14}N_2Cl_2Pt$: C, 38.41, H, 2.82, N, 5.60. Found: C, 38.88, H, 3.08, N, 5.41.

*$Pd(CNC_6H_4\text{-}p\text{-}CH_3)_2Cl_2$ (**8**).* Yield 0.062 g, 75%. ^{1}H NMR (300 MHz, CD_3CN): δ 7.44 (8H, AB, J = 8.9 Hz, C = 26 Hz), 2.41 (6H, s,

dx.doi.org/10.1021/ic301104a | *Inorg. Chem.* 2012, 51, 10728−10746

Table 2. Crystallographic Data for Complexes 9−12

	9a	9b	9c	10a
formula	$C_{16}H_{14}Cl_2N_2O_2Pt$ 0.5(CH_2Cl_2)	$C_{16}H_{14}Cl_2N_2O_2Pt$·0.25(C_6H_5Cl)	$C_{16}H_{14}Cl_2N_2O_2Pt$·0.5($C_6H_4Cl_2$)	$C_{16}H_{14}Cl_2N_2O_2Pd$
M_r	574.74	560.42	605.78	443.59
T (K)	115(2)	115(2)	115(2)	115(2)
cryst syst	triclinic	triclinic	triclinic	triclinic
space group	$P\bar{1}$	$P\bar{1}$	$P\bar{1}$	$P\bar{1}$
a (Å)	8.9518(1)	8.9948(1)	13.2283(2)	12.2899(3)
b (Å)	15.3609(2)	15.2550(2)	13.9112(2)	12.3550(3)
c (Å)	15.4429(3)	15.3945(2)	14.4607(2)	14.1451(3)
α (deg)	113.331(1)	112.743(1)	107.146(1)	96.317(1)
β (deg)	97.016(1)	97.176(1)	101.539(1)	104.314(1)
γ (deg)	100.525(1)	100.283(1)	118.042(1)	118.329(1)
V (Å^3)	1872.06(5)	1872.55(4)	2055.44(7)	1765.62(8)
Z	4	4	4	4
D_{calcd} (g cm^{-3})	2.039	1.988	1.958	1.669
μ (mm^{-1})	7.935	7.827	7.233	1.362
reflns measured	52 148	41 322	48 699	25 068
reflns unique [R_{int}]	10 028 [0.0330]	9268 [0.0341]	10 180 [0.0286]	8490 [0.0256]
reflns obsd [$I > 2\sigma(I)$]	8534	7934	9445	7194
R1, wR2 [$I > 2\sigma(I)$]	0.0186, 0.0374	0.0202, 0.0410	0.0159, 0.0354	0.0225, 0.0503
R1, wR2 (all data)	0.0271, 0.0398	0.0279, 0.0433	0.0183, 0.0361	0.0301, 0.0534

	10b	11	12
formula	$C_{16}H_{14}Cl_2N_2O_2Pd$·$C_6H_4Cl_2$	$C_{18}H_{18}Cl_2N_2Pt$	$C_{18}H_{18}Cl_2N_2Pd$
M_r	590.58	528.33	439.64
T (K)	115(2)	115(2)	115(2)
cryst syst	triclinic	triclinic	triclinic
space group	$P\bar{1}$	$P\bar{1}$	$P\bar{1}$
a (Å)	13.576(2)	8.0404(2)	8.0383(1)
b (Å)	13.705(2)	10.4016(3)	10.4097(1)
c (Å)	14.780(2)	10.8137(3)	10.7831(1)
α (deg)	76.369(9)	85.111(1)	85.4011(4)
β (deg)	64.259(8)	80.174(1)	80.3707(5)
γ (deg)	71.257(9)	87.225(1)	87.6240(5)
V (Å^3)	2330.7(6)	887.35(4)	886.353(16)
Z	4	2	2
D_{calcd} (g cm^{-3})	1.683	1.977	1.647
μ (mm^{-1})	1.277	8.207	1.348
reflns measured	63 527	19 552	14 163
reflns unique [R_{int}]	11 529 [0.0632]	4379 [0.0274]	4363 [0.0182]
reflns obsd [$I > 2\sigma(I)$]	10 129	4245	4226
R1, wR2 [$I > 2\sigma(I)$]	0.0279, 0.0708	0.0139, 0.0336	0.0158, 0.0399
R1, wR2 (all data)	0.0331, 0.0738	0.0147, 0.0339	0.0166, 0.0404

CH_3). ^{13}C NMR (101 MHz, CD_2Cl_2): δ 143.5 (s, Ar *para*), 131.0 (s, Ar *ortho*), 127.3 (s, Ar *meta*), 21.9 (CH_3); ArNC and Ar *ipso* not detected. IR (Nujol mull) ν_{max}/cm^{-1} 2253 (m), 2225 (m). Anal. Calcd for $C_{16}H_{14}N_2Cl_2Pd$: C, 46.67; H, 3.42; N, 6.86. Found: C, 46.70; H, 3.65, N, 6.68.

*Pt(CNC$_6$H$_4$-p-OMe)$_2$Cl$_2$ (**9**).* Yield 0.162 g, 78%. ^{1}H NMR (400 MHz, CD_3CN): δ 7.57 (4H, d, J = 9 Hz, *ortho* H), 7.03 (4H, d, J = 9 Hz, *meta* H), 3.84 (6H, s, OCH_3). ^{13}C NMR (151 MHz, CD_3CN): δ 162.4 (s, Ar *para*), 129.7 (s, Ar *ortho*), 119.1 (s, ArNC), 115.9 (s, Ar *meta*), 112.1 (br s, Ar *ipso*), 56.6 (OCH_3). IR (Nujol mull) ν_{max}/cm^{-1}: 2244 (m), 2213 (m). Anal. Calcd for $C_{16}H_{14}N_2O_2Cl_2Pt$·0.2CH_2Cl_2 (solvent content by ^{1}H NMR): C, 35.42, H, 2.64, N, 5.10. Found: C, 35.60, H, 2.55, N, 5.09.

*Pd(CNC$_6$H$_4$-p-OMe)$_2$Cl$_2$ (**10**).* Yield 0.088 g, 61%. ^{1}H NMR (400 MHz, CD_3CN): δ 7.59 (4H, d, J = 9 Hz, *ortho* H), 7.04 (4H, d, J = 9 Hz, *meta* H), 3.85 (6H, s, OCH_3). ^{13}C NMR (101 MHz, CD_3CN): δ 162.7 (s, Ar *para*), 129.8 (s, Ar *ortho*), 116.1 (s, Ar *meta*), 56.6 (OCH_3); ArNC and Ar *ipso* not detected. IR (Nujol mull) ν_{max}/cm^{-1}: 2238 (m), 2220 (m). Anal. Calcd for $C_{16}H_{14}N_2O_2Cl_2Pd$: C, 43.32, H, 3.18, N, 6.31. Found: C, 43.01, H, 3.30, N, 6.07.

*Pt(CNC$_6$H$_3$-2,6-Me$_2$)$_2$Cl$_2$ (**11**).* Yield 0.146 g, 86%. ^{1}H NMR (400 MHz, $CDCl_3$): δ 7.32 (2H, t, J = 7.6 Hz, *para* H), 7.18 (4H, d, J = 7.6 Hz, *meta* H), 2.50 (12H, s, CH_3). ^{13}C NMR (151 MHz, $CDCl_3$): δ 136.2 (s, Ar *ortho*), 130.8 (s, Ar *para*), 128.5 (s, *meta*), 18.8 (CH_3); ArNC and Ar *ipso* not detected. IR (KBr pellet) ν_{max}/cm^{-1}: 2229 (m), 2201 (m). Anal. Calcd for $C_{18}H_{18}N_2Cl_2Pt$: C, 40.92, H, 3.43, N, 5.30. Found: C, 40.43, H, 3.40, N, 5.37.

*Pd(CNC$_6$H$_3$-2,6-Me$_2$)$_2$Cl$_2$ (**12**).* Yield 0.116 g, 59%. ^{1}H NMR (400 MHz, CD_2Cl_2): δ 7.35 (2H, t, J = 7.6 Hz, *para* H), 7.15 (4H, d, J = 7.8 Hz, *meta* H), 2.49 (12H, s, CH_3). ^{13}C NMR (101 MHz, CD_2Cl_2): δ 136.9 (s, Ar *ortho*), 131.4 (s, Ar *para*), 128.7 (s, *meta*), 18.9 (CH_3); ArNC and Ar *ipso* not detected. IR (KBr pellet) ν_{max}/cm^{-1}: 2229 (m), 2212 (m). Anal. Calcd for $C_{18}H_{18}N_2Cl_2Pd$: C, 49.17, H, 4.13, N, 6.37. Found: C, 48.72, H, 4.14, N, 6.52.

X-ray Crystal Structure Determinations: General. X-ray diffraction data were collected on a Bruker SMART APEX II diffractometer with a CCD detector using a combination of ϕ and ω scans. The crystal-to-detector distance was 6.0 cm. A Bruker Kryoflex liquid nitrogen cooling device was used for low-temperature data collections. Unit cell determination and data collection utilized

dx.doi.org/10.1021/ic301104a | *Inorg. Chem.* 2012, 51, 10728−10746

Table 3. Metal−Metal Interactions in the Crystal Structures of $M(CNAr)_2Cl_2$ Complexes[a]

structure	M	aryl substituent	M···M (Å)	M···M···M (deg)	L_2MCl_2 stagger angle[b]
1	Pt	4-CF_3	Pt1−Pt2 3.5359(2)		139°
2	Pd	4-CF_3	Pd1−Pd2 3.5019(3)		138°
3	Pt	4-F	Pt1−Pt2 3.3747(3)		144°
			Pt1−Pt2 [1 + *x*, *y*, *z*] 3.7858(4)	Pt−Pt−Pt 143.078(9)	144°
4	Pd	4-F	Pd1−Pd2 3.3659(9)		140°
			Pd2−Pd2 [−*x*, 1 − *y*, 2 − *z*] 3.890(1)	Pd1−Pd2−Pd2 155.76(3)	180°
			Pd3−Pd4 3.4289(9)		145°
			Pd4−Pd4 [1 − *x*, 1 − *y*, 1 − *z*] 3.893(1)	Pd3−Pd4−Pd4 148.54(3)	180°
5a	Pt		Pt1−Pt1 [*x*, 1.5 − *y*, 0.5 + *z*] 3.2455(3)		139°
			Pt1−Pt1 [*x*, 1.5 − *y*, −0.5 + *z*] 3.2455(3)	Pt−Pt−Pt 160.74(2)	139°
6a	Pd		Pd1−Pd1 [*x*, 1.5 − *y*, 0.5 + *z*] 3.2370(3)		139°
			Pd1−Pd1 [*x*, 1.5 − *y*, −0.5 + *z*] 3.2370(3)	Pd−Pd−Pd 157.40(1)	139°
5b	Pt		Pt1−Pt1 [1 − *x*, 1 − *y*, 1 − *z*] 3.4001(2)		180°
6b	Pd		Pd1−Pd1 [1 − *x*, 1 − *y*, 1 − *z*] 3.3986(4)		180°
7[c]	Pt	4-Me	Pt1−Pt1 [−0.5 + *y*, 0.5 + *x*, 0.5 − *z*] 3.3393(1)		143°
			Pt1−Pt1 [−0.5 + *y*, 0.5 + *x*, −0.5 − *z*] 3.3393(1)	Pt−Pt−Pt 159.5(1)	
8[c]	Pd	4-Me	Pd1−Pd1 [−0.5 + *y*, 0.5 + *x*, 0.5 − *z*] 3.3406(1)		143°
			Pt1−Pt1 [−0.5 + *y*, 0.5 + *x*, −0.5 − *z*] 3.3406(1)	Pd−Pd−Pd 156.77(2)	
9a [**9**·0.5(CH_2Cl_2)]	Pt	4-MeO	Pt1−Pt2 3.4960(1)		140°
9b [**9**·0.25(PhCl)]	Pt	4-MeO	Pt1−Pt2 3.4726(2)		140°
9c [**9**·0.5($C_6H_4Cl_2$)]	Pt	4-MeO	Pt1−Pt2 3.2461(1)		144°
10a	Pd	4-MeO	Pd1−Pd1 [1 − *x*, 1 − *y*, 1 − *z*] 3.4643(3)		180°
10b [**10**·$C_6H_4Cl_2$]	Pd	4-MeO	Pd1−Pd2 3.5387(6)		148°
			Pd1−Pd1 [1 − *x*, 1 − *y*, 1 − *z*] 3.4947(6)	Pd1−Pd1−Pd2 157.516(9)	180°
			Pd2−Pd2 [1 − *x*, 2 − *y*, 1 − *z*] 3.5117(6)	Pd1−Pd2−Pd2 150.243(9)	180°
11	Pt	2,6-Me_2	Pt1−Pt1 [−*x*, 1 − *y*, 1 − *z*] 3.95		180°
			Pt1−Pt1 [1 − *x*, 1 − *y*, 1 − *z*] 4.13	Pt−Pt−Pt 168.8	180°
12	Pd	2,6-Me_2	Pd1−Pd1 [−x, 1 − *y*, 1 − *z*] 3.95		180°
			Pd1−Pd1 [1 − *x*, 1 − *y*, 1 − *z*] 4.12	Pd−Pd−Pd 170.0	180°

[a]From low temperature diffraction data (100−115 K) unless otherwise indicated. [b]Calculated as the average Cl−M−M−Cl dihedral angle for complexes linked by M···M interactions. [c]From data collected at 298 K.

the Bruker APEX2 software package.[33] Data integration employed SAINT.[34] Multiscan absorption corrections were implemented using SADABS.[35] X-ray diffraction experiments employed graphite-monochromated Mo Kα radiation (λ = 0.710 73 Å). Structures were solved by direct methods and refined by full-matrix least-squares on F^2 using the SHELXTL software suite.[36] Non-hydrogen atoms were assigned anisotropic temperature factors, and hydrogen atoms were included in calculated positions with fixed isotropic *U*. Face indexing of crystals to identify crystal growth axes was performed using the APEX2 software.[33] Packing interactions were identified, analyzed, and plotted using MERCURY[37] and SHELXTL/XP.[36] Specific details of structural determinations are provided below and in Tables 1 and 2.

*X-ray Crystal Structures of Pt/Pd(CNC_6H_4-p-CF_3)$_2Cl_2$ (**1**, **2**).* The CF_3 group of C47 in each structure was treated as rotationally disordered between two orientations using a two-part model for F10, F11, and F12. The refined occupation ratios of the two orientations were 0.59:0.41 for **1** and 0.81:0.19 for **2**. Least-squares restraints were employed to attain reasonable thermal parameters on these F atoms.

*X-ray Crystal Structure of Pt(CNC_6H_4-p-F)$_2Cl_2$ (**3**).* With the aid of ROTAX[38] the crystal used to obtain 115 K data was modeled as a two-component pseudomerohedral twin (twin law: 1 0 0, 0 −1 0, 0 0 −1). The refined proportion of the twin components was 0.689(1):0.311(1). The crystal used for room temperature structure determination did not exhibit twinning.

*X-ray Crystal Structure of Pd(CNC_6H_4-p-F)$_2Cl_2$ (**4**).* With the aid of CELL_NOW[39] and TWINABS,[40] a crystal of **4** was modeled as a two-component nonmerohedral twin.[41] For 36 222 reflections in the scaled data set, 6.5% were singles assigned to twin component 1, 6.5% were singles assigned to component 2, and 87% were composite reflections. Final refinement was performed on both twin components using data in HKLF5 format. The refined proportion of twin components was 0.457(1):0.543(1), with a refined twin law of −1 0 0, 0 −1 0, 0.56 0.56 1.

*X-ray Crystal Structures of Pt/Pd(CNC_6H_4-p-CH_3)$_2Cl_2$ (**7**, **8**).* Crystals of **7** and **8** gave diffraction patterns indicative of severe twinning at 115 K, and standard twin deconvolution procedures failed to produce solvable data sets. Room temperature data did not show these problems, suggesting that a phase change destroyed the integrity of the crystals at low temperatures. Final data were collected at 298 K. To correct for electron density arising from disordered solvent, diffraction data were treated with the SQUEEZE procedure in PLATON.[42] SQUEEZE analyses were consistent with 20 H_2O molecules per unit cell in the sample of **7** examined and 13 molecules of H_2O per unit cell in the sample of **8** examined.

*X-ray Crystal Structures of M(CNC_6H_4-p-OCH_3)$_2Cl_2$·x(solvent) (**9a−c**, **10b**).* Discrete solvent molecules were located in the difference Fourier maps of **9a−c** and **10b** and refined as part of the structural models. In the case of **9b**, the chlorobenzene molecule was modeled as disordered between two orientations related by an inversion center in a 50:50 occupancy ratio. Appropriate least-squares restraints were applied to aid refinement of the PhCl molecule.

Temperature Dependence of Unit Cell Parameters. For samples of **3**, **5a**, and **7**, limited data sets were collected at five 50 K increments from 300 to 100 K. Samples were allowed to equilibrate for three hours at each temperature before data were collected. At each temperature, a set of 200−350 diffraction images was obtained, and cell parameters were refined using SAINT.[34]

Photophysical Measurements. Steady-state luminescence spectra were acquired with a PTI QuantaMaster model QM-4 scanning spectrofluorometer equipped with a 75-W Xe lamp, emission and excitation monochromators, excitation correction unit, and a PMT detector. The emission and excitation spectra were corrected for the

dx.doi.org/10.1021/ic301104a | Inorg. Chem. 2012, 51, 10728−10746

wavelength-dependent detector response and Xe lamp intensity, respectively. Temperature dependent studies were acquired with an Oxford optical cryostat using liquid helium or liquid nitrogen as coolant. Lifetime data were acquired using a nitrogen laser interfaced with a tunable dye laser and a frequency doubler, as part of fluorescence and phosphorescence subsystem add-ons to the PTI instrument. The 337.1 nm line of the N_2 laser was used to pump a freshly prepared 1×10^{-2} M solution of the organic continuum laser dye Coumarin-540A in ethanol, the output of which was tuned and frequency doubled to attain the suitable excitation wavelength (based on the steady-state luminescence excitation spectra) used to generate the time-resolved data. Absorption spectra were acquired with a Cary 100 double-beam UV–vis spectrophotometer for dilute solutions of complexes in freshly distilled CH_2Cl_2.

RESULTS AND DISCUSSION

Crystallographic Studies. This study focused on a series of 4-substituted phenyl isocyanides (R = CF_3, F, Me, OMe) in order to vary the isocyanide electronic properties with minimal steric perturbation (complexes **1**–**4** and **7**–**10**, Chart 1). Complexes of 2,6-dimethylphenyl isocyanide (**11**, **12**) were also prepared in order to examine how increased steric bulk near the metal would affect the solid-state structure.[43,44] Initial crystal growth attempts utilized slow diffusion of *n*-hexane into concentrated CH_2Cl_2 solutions of the complexes. If no X-ray quality crystals were obtained, further attempts were made using slower diffusing solvent pairs such as cyclohexane/chlorobenzene.

Metal–metal contacts are compiled in Table 3. A summary of all observed packing interactions is given in Table 4, and a complete tabulation is provided in Table S1 (Supporting Information). All π–π interactions with interplanar spacings less than 3.8 Å are considered to be significant.[8,15j] For purposes of discussion, π–π interactions involving overlap of at least $^1/_3$ of the adjacent rings are designated as "offset", whereas those involving a single edge of each ring are described as "peripheral". Note that these categories do not correlate clearly with ring centroid–centroid distances, as the interplanar spacings (and angles, for nonparallel contacts) vary significantly.[8]

Table 4. Average Number of Metal–Metal, π–π, and Other Packing Interactions per Complex

structure	# M···M ≤ 3.4 Å	# M···M 3.5–4.1 Å	# π–π	other
1	0	1	1.5	1 CF_3–π
				1 Pt–π
2	0	1	1.5	1 CF_3–π
				1 Pd–π
3	1	1	4	
4	1	0.5	4	
5a	2	0	2	2 CH–π
5b	1	0	1	2 CH–π
6a	2	0	2	2 CH–π
6b	1	0	1	2 CH–π
7	2	0	2	2 CH_3–π
8	2	0	2	2 CH_3–π
9a	0	1	1.5	3 CH_3–π
9b	0	1	1.5	3 CH_3–π
9c	1	0	2	1.5 CH–π
				1 CH_3–π
10a	0	0.5	2.5	2 CH_3–π
10b	0	2	2.5	1 CH–π
				1 CH_3–π
11	0	2	0	4 CH_3–π
12	0	2	0	4 CH_3–π

Structures of 1 and 2, Pt/Pd(CNC_6H_4-*p*-CF_3)$_2Cl_2$. Slow diffusion of cyclohexane into chlorobenzene solutions of **1** and **2** led to formation of X-ray quality crystals. The structure of Pt(CNC_6H_4-*p*-CF_3)$_2Cl_2$ (**1**) has an asymmetric unit consisting of two crystallographically nonequivalent complexes linked by a Pt1···Pt2 contact of 3.5359(2) Å (Table 3). This distance is in the expected range for a van der Waals contact,[45] suggesting a weak contribution, if any, from metallophilic bonding. A second packing motif is aryl π–π stacking. The C21 ring[46] of the Pt1 complex forms a slightly offset π–π interaction with the C41 ring of a Pt2 complex in a neighboring asymmetric unit, with the two CF_3 groups oriented approximately 60° apart. The C41 ring, in turn, is involved in a slightly offset π–π interaction with an inversion-related C41 ring, but with the CF_3 groups oriented 180° apart. The combination of these π–π interactions results in a four-ring π-stack (center, Figure 1). A third type of packing interaction comprises CF_3–π interactions between inversion-related pairs of C31 rings on the Pt2 complex. The C31 rings do not directly overlap, instead adopting a parallel orientation with the *p*-CF_3 groups projecting over the adjacent rings (red dashes, Figure 1). One F atom of each of these CF_3 groups (F8) exhibits a close contact with the adjacent C31 ring, lying 3.13 Å from the plane of the ring and 3.20 Å from the ring centroid.

Metallophilic contacts are limited to isolated interactions between two complexes, with no extended Pt···Pt chains. On the face of the square plane opposite the Pt1···Pt2 contact, Pt2 is "capped" by an apparent metal–π interaction[10] with the C11 ring of a neighboring Pt1 complex. No such interaction is seen for Pt1.

The palladium congener Pd(CNC_6H_4-*p*-CF_3)$_2Cl_2$ (**2**) crystallizes in the same space group as **1** and has very similar unit cell parameters (Table 1). All of the packing interactions observed for **1** are also present for **2** (Figure S1, Supporting Information). The Pd1···Pd2 distance is slightly shorter at 3.5019(3) Å, reflecting the slightly smaller van der Waals radius of Pd versus Pt.[45] All of the interplanar and intercentroid distances for arene π–π and related interactions are within 0.1 Å of those seen for **1**.

Structures of 3 and 4, Pt/Pd(CNC_6H_4-*p*-F)$_2Cl_2$. Long rods of Pt(CNC_6H_4-*p*-F)$_2Cl_2$ (**3**) were obtained by slow diffusion of the *n*-hexane/CH_2Cl_2 solvent pair. Similarly to **1**, the structure of **3** has two crystallographically nonequivalent complexes per asymmetric unit. A Pt1···Pt2 contact of 3.3747(3) Å is present between the two complexes (Table 3). This distance is less than the sum of van der Waals radii and thus consistent with metallophilic bonding. These dimers are linked by substantially longer interdimer Pt2···Pt1 contacts of 3.7858(4) Å, resulting in extended zigzag chains of alternating long and short Pt···Pt interactions along the crystallographic *a* axis (Figure 2a). These chains are interdigitated with adjacent chains related by a 2_1 screw axis along *b* through peripheral π–π interactions. These π–π interactions repeat along the *a* direction, forming extended C11–C41–C11–C41 and C21–C31–C21–C31 stacks with interplanar separations of 3.31–3.41 Å. The combination of Pt···Pt π–π interactions results in two-dimensional sheets of interlinked complexes parallel to the *ab* plane (Figure 3a). The nearly coplanar arrangement of aryl rings in each complex appears to facilitate the synergistic combination of these two interactions. Along the *c* direction,

dx.doi.org/10.1021/ic301104a | *Inorg. Chem.* 2012, 51, 10728–10746

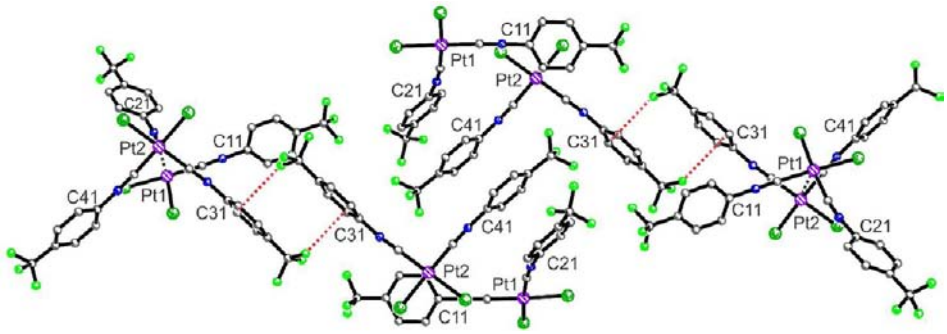

Figure 1. Partial packing diagram of **1**, showing Pt···Pt interactions, aryl $\pi-\pi$ stacking interactions (center), and $CF_3-\pi$ interactions (red dashes).

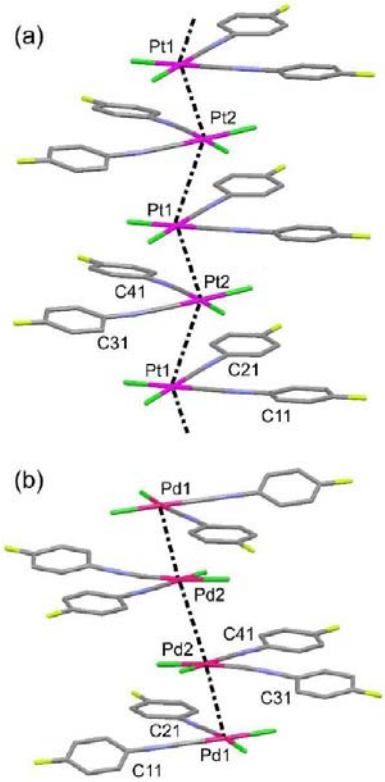

Figure 2. Comparison of M···M interactions in 4-fluorophenyl isocyanide complexes. (a) Portion of an extended Pt···Pt chain in the crystal structure of **3**. View is approximately down the *c* axis. (b) One of the dimers-of-dimers present in **4**. A crystallographically independent second dimer-of-dimers (Pd3/Pd4) is shown in Figure S3 (Supporting Information).

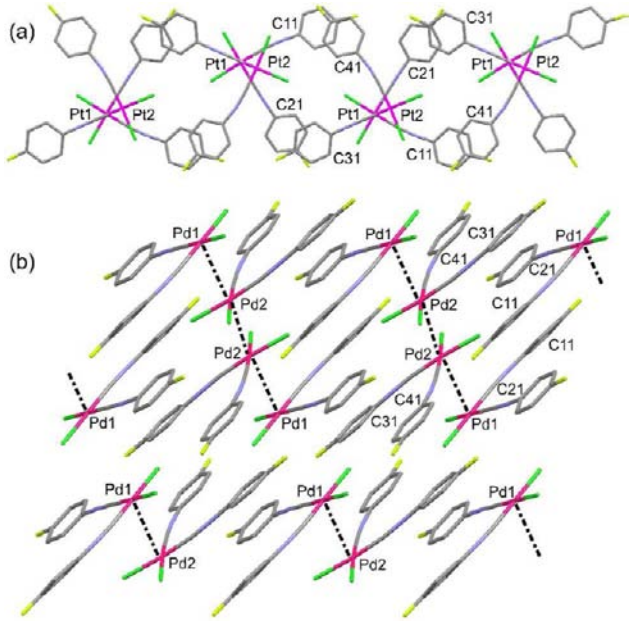

Figure 3. Crystal packing in 4-fluorophenyl isocyanide complexes. (a) View down the Pt···Pt chains of **3**, showing interlinking via $\pi-\pi$ interactions to form two-dimensional sheets. (b) Side view of a sheet formed by $\pi-\pi$ stacking interactions between dimers-of dimers in **4**. Similar sheets formed by Pd3/Pd4 complexes are shown in Figure S4 (Supporting Information).

adjacent sheets pack only through van der Waals contacts between aryl rings and/or Cl ligands (Figure S2, Supporting Information).

For the palladium analogue $Pd(CNC_6H_4\text{-}p\text{-}F)_2Cl_2$ (**4**), identical crystal growth conditions led to a structure that is notably different from **3**. The asymmetric unit of **4** contains two pairs of associated Pd complexes, for a total of four crystallographically independent molecules. The two pairs of complexes form two separate but similar supramolecular assemblies. Pd1 and Pd2 are separated by a short distance of 3.3659(9) Å. This pair is linked into a "dimer-of-dimers" through a longer contact of 3.890(1) Å between Pd2 and its inversion-related symmetry equivalent, resulting in a short–long–short M···M contact motif similar to that seen in **3**, but with the contacts running approximately along the [110] lattice direction (Figure 2b). Unlike **3**, the metal–metal contacts do not form extended chains. The dimers-of-dimers are slipped along *c* relative to the nearest neighboring stack, and the closest Pd1···Pd1 contact is 5.93 Å. The isocyanide aryl groups are nearly parallel to the metal coordination plane as in **3**, facilitating a network of peripheral $\pi-\pi$ stacking interactions. However, every third complex in a stack is rotated by approximately 30°, unlike the eclipsed arrangement of every other complex in **3**, so the resulting $\pi-\pi$ stacking pattern is more complex. Each dimer-of-dimers is linked via $\pi-\pi$ interactions to the two neighboring stacks in the positive and negative *a* direction and to two other inversion-related stacks (Figure 3b). The result is two-dimensional sheets of interlinked dimers-of-dimers parallel to the *ab* plane. The Pd3–Pd4 pair of complexes forms an analogous sheet structure with Pd3 replacing Pd1 and Pd4 replacing Pd2 (Figure S4, Supporting Information). The Pd1–Pd2 sheets alternate with Pd3–Pd4 sheets along the *c* axis, with only van der Waals contacts linking them. A further difference from **3** is that the Pd3 and Pd4 complexes are canted in the opposite direction from the Pd1

dx.doi.org/10.1021/ic301104a | *Inorg. Chem.* 2012, 51, 10728–10746

and Pd2 complexes, forming a herringbone-like arrangement of the alternating sheets (Figure S5, Supporting Information). The distinct packing arrangement of **4** results in a slightly higher packing index (68.8%) relative to the Pt analogue **3** (68.1%),[47] apparently at the expense of extended metal−metal interactions.

Structures of 5a and 6a, Chain Form of Pt/Pd-$(CNC_6H_5)_2Cl_2$. As previously communicated, crystal growth of $M(CNC_6H_5)_2Cl_2$ from *n*-hexane/CH_2Cl_2 provided long yellow rods of the chain forms **5a**/**6a**, whereas slower crystal growth from chlorobenzene/cyclohexane afforded the dimer polymorphs **5b**/**6b**.[19] Compounds **5a** and **6a** feature extended zigzag chains of metal atoms with short M···M contacts (Figure 4), two "bands" of $\pi-\pi$ interactions (Figure 5a), and void

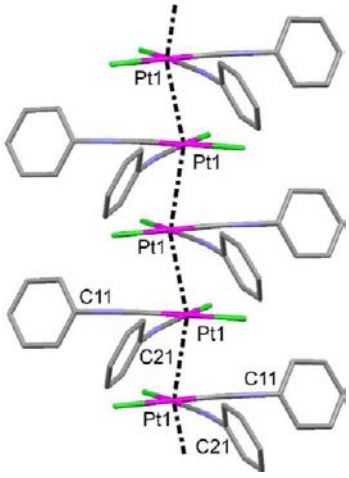

Figure 4. Portion of a Pt···Pt chain in the crystal structure of **5a**. View is approximately down the *a* axis. A comparable view of the Pd analogue **6a** is shown in Figure S6 (Supporting Information).

channels parallel to the metal chains (Figure 5b). The channels are walled by phenyl rings, which are canted relative to the metal coordination plane at dihedral angles of 65−73°. Also apparent is a CH···π contact between the *para* hydrogen of each C21 ring and the *ipso* carbon of an adjacent C11 ring. These interactions form part of the walls of the channels (Figure 5b).

Structures of 5b and 6b, Dimer Form of Pt/Pd$(CNC_6H_5)_2Cl_2$. The dimer polymorphs **5b** and **6b** contain only isolated M···M contacts of 3.40 Å, significantly longer than those in the chain polymorphs. Only one $\pi-\pi$ interaction occurs per complex: an offset interaction between C21 rings of inversion-related complexes (Figure 6). A pair of CH···π contacts between the *para* hydrogens of the C21 rings and C11 on the opposite complex reinforces these $\pi-\pi$ interactions. All other crystal packing occurs through nonspecific molecular contacts. The more efficient overall packing in **5b**/**6b** (respective packing indices 67.6% and 67.3%) versus **5a**/**6a** (packing indices 63.1% and 63.5%),[48] albeit at the expense of extended M···M contacts, is facilitated by a different orientation of the Ph rings. They are canted in the same direction at dihedral angles of 64−67°, in contrast to the disrotatory arrangement seen in **5a**/**6a**.

Structures of 7 and 8, Pt/Pd$(CNC_6H_4$-*p*-$CH_3)_2Cl_2$. Long yellow rods of **7** and **8** formed upon slow diffusion of cyclohexane into chlorobenzene solutions of the complexes. Crystals of both complexes showed near-identical unit cell

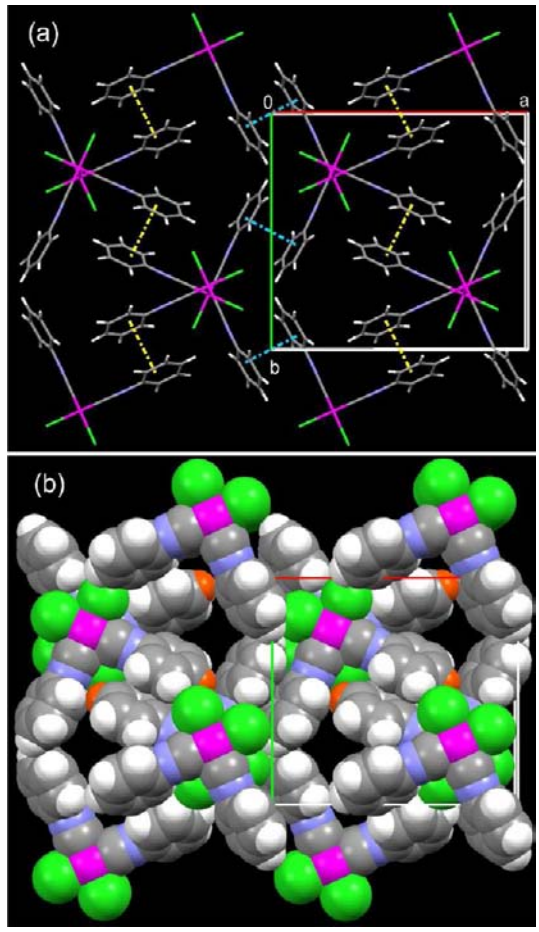

Figure 5. (a) View along the *c* axis of **5a**, showing aryl $\pi-\pi$ interactions between C11 rings (blue dashes) and C21 rings (yellow dashes). (b) Space-filling view along the *c* axis, showing empty channels at ($^1/_4$, $^3/_4$, *z*) and ($^3/_4$, $^1/_4$, *z*) and CH−π interactions (orange). A comparable view of the Pd analogue **6a** is shown in Figure S7 (Supporting Information).

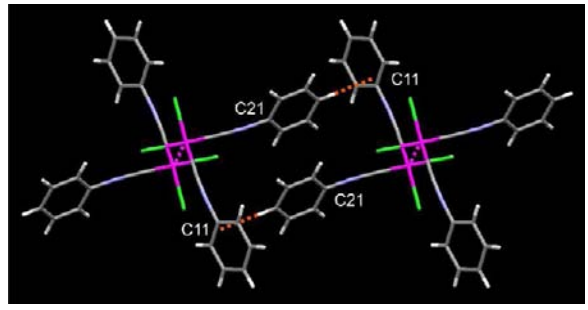

Figure 6. View of two dimers of **5b** linked by $\pi-\pi$ (center) and CH−π (orange dash) interactions. A comparable view of the Pd analogue **6b** is shown in Figure S8 (Supporting Information).

parameters and molecular packing arrangements. All non-hydrogen atoms except the *ortho* and *meta* carbons are located on a crystallographic mirror plane. The *p*-tolyl rings are rotated to dihedral angles of exactly 90° relative to the coordination plane. Adjacent complexes related by a *c* glide are staggered at approximate angles of 143°, similar to the arrangement seen in **5a**/**6a**. This allows them to form zigzag chains of metallophilic interactions along the *c* axis, with uniform M···M contacts of 3.34 Å (Figure 7). Each complex also forms slightly offset $\pi-\pi$

dx.doi.org/10.1021/ic301104a | *Inorg. Chem.* 2012, 51, 10728−10746

interactions with the C11 and C21 rings of two complexes related by a 4-fold rotation axis (Figure 8).

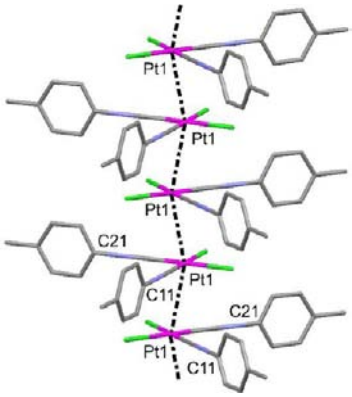

Figure 7. Portion of a Pt···Pt chain in the crystal structure of **7**. View is approximately perpendicular to the *c* axis. A comparable view of the Pd analogue **8** is shown in Figure S9 (Supporting Information).

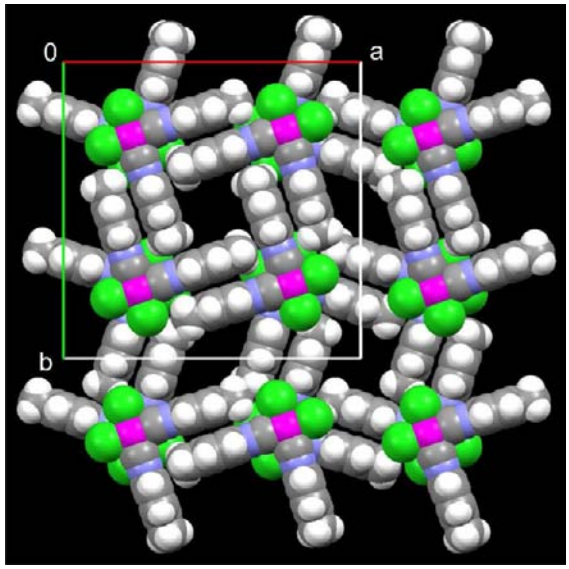

Figure 8. View along the *c* axis of **7**. Square channels are apparent at ($^1/_2$, $^1/_2$, *z*) and (1, 1, *z*), and rhombic channels are visible at (1, $^1/_2$, *z*) and ($^1/_2$, 1, *z*). A comparable view of the Pd analogue **8** is shown in Figure S10 (Supporting Information).

The combination of M···M and $\pi-\pi$ packing interactions results in two sets of infinite channels running parallel to the M···M chains (Figure 8). Channels of the first set are square-shaped and centered on 4-fold rotation axes, with the channel walls formed by C21 aryl rings. The methyl group of each C21 ring forms a a $CH_3\cdots\pi$ interaction[49,50] with the *ipso* carbon on the adjacent wall of the channel, creating a whorl-like arrangement. The second set consists of rhombic channels walled by C11 aryl rings. The square channels have minimum channel widths of 4.6 Å between opposite walls and maximum diagonal widths of 5.9 Å, accounting for the van der Waals radii of atoms lining the channels. The rhombic channels have minimum widths of 3.9 Å and maximum widths of 7.6 Å. Both types of channel are significantly larger than the 3−4 Å wide channels of **5a**/**6a** and occupy a larger portion of the unit cell volume: 20%, versus 11% for **5a**/**6a**. Unlike the empty channels of **5a**/**6a**, the channels of **7** and **8** contain a significant amount of solvent as judged by the presence of difference Fourier peaks. Attempts to model this electron density as discrete molecules of solvents used in synthesis or crystallization were unsuccessful. Assignment of peaks as partially occupied oxygen atoms led to reasonable refinement, but physically meaningful arrangements of water molecules were not identified. Therefore, the SQUEEZE procedure[42] was utilized to correct the structural data for the disordered electron density (see the Experimental Section). Although the amount of water in the channels appeared to vary for different samples, the two types of channels contained roughly equal amounts of disordered electron density in each case.

Structures of 9a−c, $Pt(CNC_6H_4$-*p*-$OCH_3)_2Cl_2\cdot x$(solvent). Large crystals were obtained both by diffusion of an Et_2O/*n*-hexane mixture into a CH_2Cl_2 solution of **9** and by diffusion of cyclohexane into a chlorobenzene solution of **9**. The two types of crystal have nearly identical unit cell parameters and packing arrangements and differ only in the identity of the occluded solvent: 0.5 molecule of CH_2Cl_2 per Pt in the first case (**9a**) and 0.25 molecule of chlorobenzene in the second case (**9b**).

The asymmetric units of **9a** and **9b** consist of two independent complexes joined by Pt···Pt contacts of 3.50 Å (**9a**, Figure 9) or 3.47 Å (**9b**, Figure S11, Supporting Information). Two types of $\pi-\pi$ interaction are present: peripheral interactions between the C11 and C21 rings of inversion-related Pt1 complexes, and offset stacking between the C31 rings of inversion-related Pt2 complexes. The steric demands of the OCH_3 substituents appear to hinder extensive $\pi-\pi$ stacking and reduce the efficiency of the observed $\pi-\pi$ interactions. In particular, the interaction between the C11 and C21 rings deviates significantly from a parallel arrangement (dihedral angle 15−16°). In addition, three $CH_3\cdots\pi$ interactions are apparent, with one CH_3 hydrogen atom located 2.8−3.3 Å from the centroid of a neighboring aryl ring in each case (Figure 9a, Table S1).

The occluded solvents in **9a**,**b** occupy channels that run along the *a* axes (Figure 9b). The channels appear to be stabilized by a combination of Pt···Pt dimer formation, $\pi-\pi$ stacking, and $CH_3\cdots\pi$ interactions, with no specific packing motif dominating. Unlike the channeled structures of **5a**/**6a** and **7**/**8**, there are no extended M···M interactions in **9a**,**b**. The Pt square planes are tilted relative to the channel axis instead of being perpendicular as in **5a**/**6a** and **7**/**8**. The maximum continuous widths of the channels are only 3.2 Å, but they contain deeper indentations that allow them to accommodate solvent molecules. The channel walls are not lined by aryl ring π-systems as in **5a**/**6a**, but rather by chloride ligands and aryl ring peripheries. The channels occupy 11% of the unit cell volume in **9a** and **9b**, similarly to the vacant channels of **5a**/**6a**.

Crystals of **9** were also grown by slow diffusion of cyclohexane into a 1,2-dichlorobenzene solution of the complex in an attempt to prepare a solvent-free crystalline form. Instead, a new solvate structure (**9c**) containing 0.5 equiv of *o*-$C_6H_4Cl_2$ per Pt was obtained. As in **9a**,**b**, the asymmetric unit contains two complexes joined by a Pt···Pt contact. The two complexes in **9c** pack more closely than those in **9a**,**b**, giving a shorter Pt···Pt distance of 3.25 Å, despite being staggered at a similar angle (143°, versus 140° for **9a**,**b**). This does not appear to result from any single factor, but rather from the cumulative effects of a different array of packing interactions.

The solvent molecules do not occupy channels in **9c**, but rather occur as $\pi-\pi$ stacked dimers that are "boxed in" by the C21, C31, and C41 aryl rings (Figure 10). The *o*-$C_6H_4Cl_2$

dx.doi.org/10.1021/ic301104a | *Inorg. Chem.* 2012, 51, 10728−10746

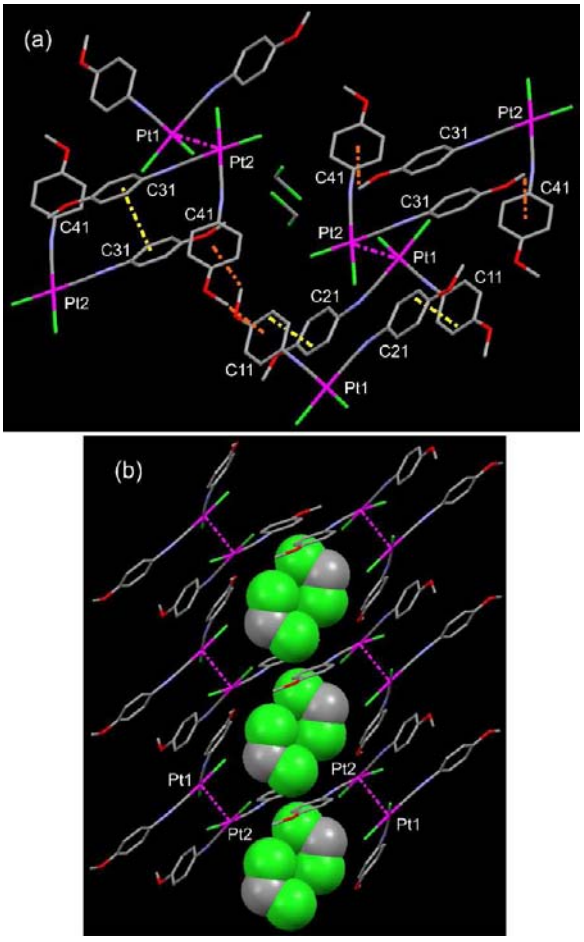

Figure 9. (a) Partial packing diagram of **9a**, showing Pt···Pt contacts (magenta dashes), $\pi-\pi$ interactions (yellow dashes), and $CH_3-\pi$ interactions (orange dashes). View is along a CH_2Cl_2-filled channel (center) running along the *a* axis. (b) View perpendicular to the solvent-filled channels of **9a**, with CH_2Cl_2 molecules shown in a space-filling representation. Comparable views of the chlorobenzene solvate **9b** are shown in Figure S11 (Supporting Information).

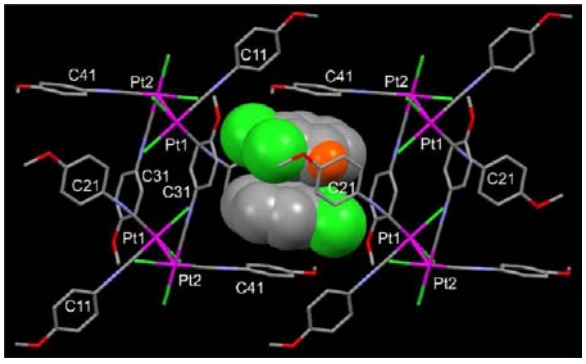

Figure 10. Packing of Pt complexes around a $\pi-\pi$ stacked pair of 1,2-dichlorobenzene solvent molecules in **9c**. A CH- interaction (orange) and a portion of the extended C41-solvent−solvent-C41 $\pi-\pi$ stacking interactions (center) are shown. Additional packing views of **9c** are shown in Figures S12 and S13 (Supporting Information).

solvent engenders more extensive $\pi-\pi$ stacking than is seen in **9a,b**. The *o*-$C_6H_4Cl_2$ dimers form $\pi-\pi$ interactions with the C41 rings of Pt2 complexes, which in turn engage in peripheral $\pi-\pi$ stacking with the C41 rings of neighboring complexes. These stacks continue infinitely along the [111] lattice direction (Figure S12, Supporting Information). The aryl rings of the Pt2 complex are rotated at dihedral angles of 76° and 88° relative to the coordination plane in order to accommodate these $\pi-\pi$ interactions. The Pt1 complex forms peripheral $\pi-\pi$ interactions with an inversion-related Pt1 complex through both the C11 and C21 rings. There is less involvement of $CH_3\cdots\pi$ interactions compared to **9a,b**, with only one example involving the C31 ring. However, two aryl CH···π contacts are present, one between neighboring complexes (C41 and C11 rings) and one between the *o*-$C_6H_4Cl_2$ solvent and the C21 ring of a complex (Figure 10 and Figure S13, Supporting Information).

Structures of Pd(CNC$_6$H$_4$-*p*-OCH$_3$)$_2$Cl$_2$·(10a) and 1,2-Dichlorobenzene Solvate (10b). In contrast to **9**, slow diffusion of *n*-hexane into CH_2Cl_2 solutions of **10** produced a solvent-free form of the compound (**10a**). The two crystallographically independent complexes of **10a** are oriented with their coordination planes in a nonparallel arrangement (dihedral angle 69°), precluding any close Pd1···Pd2 contacts. Each Pd1 complex forms a head-to-tail dimer with an inversion-related complex at a Pd1···Pd1 distance of 3.46 Å (Figure 11).

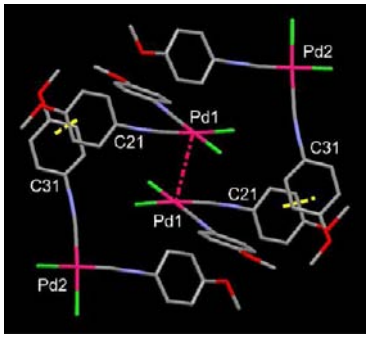

Figure 11. View of a Pd1 dimer in **10a**, showing Pd···Pd contact (pink dash) and aryl $\pi-\pi$ interactions with Pd2 complexes (yellow dashes). Additional packing interactions of **10a** are shown in Figure S14 (Supporting Information).

The Pd2 complexes do not form any short Pd···Pd interactions. The orientations of the aryl rings also differ relative to **9a−c**. Both rings are nearly parallel to the coordination plane for the Pd2 complex, but one of the rings (C21) is rotated by 67° in the Pd1 complex. This allows the C21 ring to form offset $\pi-\pi$ stacking interactions with the C31 and C41 rings of two neighboring Pd2 complexes. In combination with peripheral $\pi-\pi$ contacts between inversion-related C31 rings, these interactions form 6-ring π stacks that run along the [011] direction. The C11 ring of the Pd1 complex does not exhibit any $\pi-\pi$ interactions, but it is involved in two $CH_3\cdots\pi$ interactions, one with an inversion-related C11 ring and one with the C21 ring of a neighboring Pd1 complex (Figure S14, Supporting Information).

Crystal growth of **10** using the 1,2-dichlorobenzene/*n*-hexane solvent pair, under conditions identical to those used to obtain **9c**, led to a $C_6H_4Cl_2$ solvate (**10b**) that is different from **9c**. Like **9c**, **10b** has two crystallographically independent complexes linked by a Pd···Pd interaction, but there are also two independent $C_6H_4Cl_2$ molecules, giving a 1:1 Pd/solvent ratio, in contrast to the 2:1 Pt/solvent ratio in **9c**. The Pd1···Pd2 dimers form infinite chains of Pd···Pd interactions (Figure 12), although these are significantly longer than the

dx.doi.org/10.1021/ic301104a | *Inorg. Chem.* 2012, 51, 10728−10746

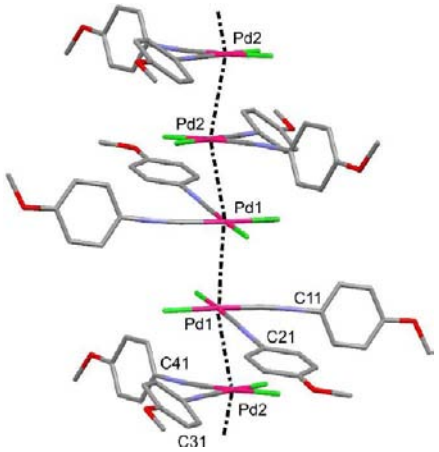

Figure 12. Portion of a Pd···Pd chain in the crystal structure of **10b**. View is approximately perpendicular to the *b* axis.

isolated Pt···Pt contacts of 3.25 Å in **9c**. Each Pd1 and Pd2 forms a head-to-tail interaction with an inversion-related complex, with respective Pd1···Pd1 and Pd2···Pd2 distances of 3.49 and 3.51 Å. The Pd1···Pd2 contacts are longer at 3.54 Å, despite the stagger angle (148°) being similar to those in structures such as **5a**/**6a** and **9c** with shorter M···M distances. The Pd1 and Pd2 complexes appear to be pushed slightly apart to accommodate other packing interactions.

As in **9c**, the $C_6H_4Cl_2$ solvent molecules in **10b** facilitate $\pi-\pi$ interactions, but to an even greater extent. Each of the two $C_6H_4Cl_2$ molecules forms a $\pi-\pi$ stacked dimer with an inversion-related molecule, with each dimer surrounded by isocyanide aryl rings. Both dimers are incorporated into infinite stacks of $\pi-\pi$ interactions running roughly perpendicular to the Pd···Pd chains, with solvent dimers alternating with $\pi-\pi$-stacked pairs of inversion-related aryl rings (Figure 13). These π stacks occur in layers involving only the C11 rings of the Pd1 complexes or only the C41 rings of the Pd2 complexes for the two independent sets of solvent molecules. Offset $\pi-\pi$ contacts involving inversion-related C21 rings also occur in the Pd1 layers (Figure 13), whereas $CH_3\cdots\pi$ interactions between inversion-related C31 rings exist in the Pd2 layers (Figure S15, Supporting Information). Oblique $CH-\pi$ interactions link the C21 rings in the Pd1 layers to C31 rings in the adjacent Pd2 layers (Figure S16).

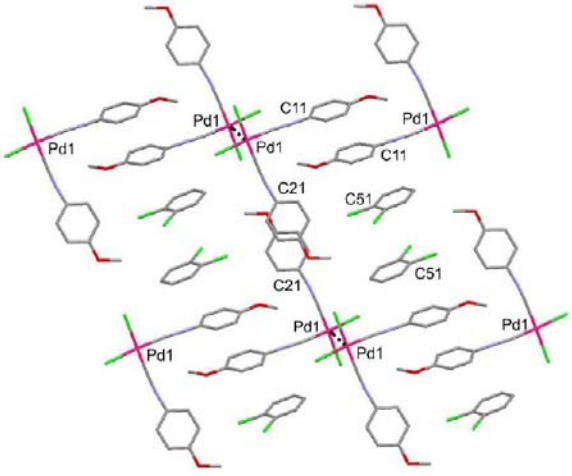

Figure 13. Packing diagram of the Pd1 layer of **10b**, showing extended stacks of C11−C11-dichlorobenzene−dichlorobenzene $\pi-\pi$ interactions and an isolated C21−C21 $\pi-\pi$ interaction (center). View is approximately down the *b* axis, and the extended $\pi-\pi$ stacking runs along the *c* axis. Packing in the Pd2 layer and between layers is shown in Figures S15 and S16 (Supporting Information).

Structures of 11 and 12, Pt/Pd(CNC_6H_3-2,6-Me_2)$_2Cl_2$. Crystals of **11** and **12** were obtained by diffusion of *n*-hexane into CH_2Cl_2 solutions of the compounds. The structures of **11** and **12** are nearly identical. The complexes form infinite stacks along the *a* axis, with adjacent complexes adopting a near head-to-tail orientation that is slightly laterally offset to accommodate steric interactions between the bulky aryl groups (Figure 14).

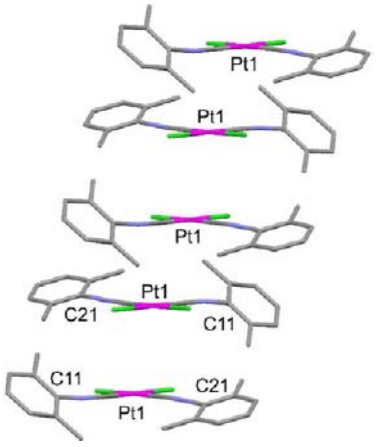

Figure 14. Extended head-to-tail stacking in the crystal structure of **11**. Pt···Pt distances alternate between 3.95 Å (bottom two complexes) and 4.13 Å. A comparable view of the Pd analogue **12** is shown in Figure S17 (Supporting Information).

The alternating M···M distances of 3.95 and 4.12−4.13 Å are too long to signify significant metallophilic interactions. The steric demands of the aryl rings apparently preclude any $\pi-\pi$ interactions. However, neighboring stacks along the *b* and *c* axes are linked via reciprocal $CH_3\cdots\pi$ interactions between inversion-related C11 and C21 rings, respectively (Figures S18 and S19, Supporting Information).

Discussion of Crystal Packing Interactions. Table 4 divides observed M···M contacts into short interactions likely to have some contribution from metallophilic bonding, and longer ones where the proximity of the metal atoms may be a fortuitous result of other interactions. The dividing line of 3.4 Å is twice the van der Waals radius of Pt.[45] The M···M distances range from 3.24 to 3.25 Å for **5a**/**6a** and **9c** to 3.95−4.13 Å for **11**/**12**. All interactions less than 3.4 Å exhibit a staggered geometry, with adjacent complexes rotated by angles of 138−144° (last column, Table 3). This arrangement appears to minimize steric interactions between the ligands, thereby facilitating close contacts between the metal atoms. By contrast, many of the longer interactions (i.e., those in **4**, **10a**, **10b**, and **11**/**12**), as well as the borderline 3.40 Å contacts of **5b**/**6b**, feature a head-to-tail arrangement of complexes with a rotation angle of 180°. This geometry is more plausibly ascribed to interactions of molecular dipoles than to orbital-based M···M interactions. However, several longer interactions (i.e., those in **1**/**2**, **3**, **9a**, **9b**, and Pd1···Pd2 in **10b**) show staggered geometries. This suggests that formation of both optimal M···M contacts and dipole−dipole interactions may be

dx.doi.org/10.1021/ic301104a | *Inorg. Chem.* 2012, 51, 10728−10746

prevented by ligand steric properties or the need to accommodate other packing interactions.

There is no clear correlation between the degree of metal−metal interaction and the electronic properties of the arylisocyanide substituents. The most extensive metal−metal contacts are seen for **5a**/**6a** and **7**/**8**, both of which contain zigzag chains with two short contacts per metal atom. Although electron-releasing substituents could hypothetically enhance metallophilic bonding by increasing the degree of configuration interaction,[7] the metal−metal contacts are actually longer in **7**/**8** (R = *p*-CH_3, Hammett $\sigma = -0.14$)[51] than in **5a**/**6a** (R = H, $\sigma = 0$). Furthermore, structures containing the electron-releasing *p*-OMe substituent (**9a**−**c** and **10a**,**b** ; $\sigma = -0.29$) showed only isolated M···M contacts, all of them longer than 3.4 Å except for the 3.25 Å Pt···Pt distance of **9c**. The complexes with the strongest electron-withdrawing substituents, **1**/**2** (R = *p*-CF_3, $\sigma = 0.53$), show a similar degree of metal−metal contact to the *p*-OMe structures, with only isolated M···M distances of ∼3.5 Å. The sterically hindered complexes **11**/**12** (R = 2,6-Me_2) exhibit only longer head-to-tail contacts (≥4.0 Å) that preclude any metallophilic interactions.

The overall pattern suggests that substituents with smaller steric demands generally lead to increased metallophilic contacts. However, Pt complex **3** (R = *p*-F, $\sigma = 0.15$) provides some evidence that electron-withdrawing groups may reduce the tendency for M···M interactions to form. Complexes with phenyl isocyanide (**5a**) and bulkier but more electron-rich *p*-tolyl isocyanide (**7**) are both able to accommodate extended chains of short Pt···Pt contacts. The steric bulk of a *p*-F substituent falls between those of H and Me, so it is likely that an extended chain structure would be feasible for **3** as well. Instead, **3** adopts a structure intermediate between an extended chain and isolated dimers, with short, staggered Pt···Pt contacts alternating with longer ones. Notably, the number of aryl $\pi-\pi$ interactions is increased in **3** relative to **5a** and **7** (Table 4).

It is evident that $\pi-\pi$ and related packing interactions can either disrupt M···M interactions or synergistically stabilize them. Both structures with extended chains of short M···M contacts, **5a**/**6a** and **7**/**8**, exhibit two $\pi-\pi$ interactions and two CH···π contacts per complex. Thus, it seems likely that these π interactions play an important role in stabilizing the aryl-walled channels in these two structure types. Aryl $\pi-\pi$ interactions reach a maximum of four per complex in **3** and **4**, in which the *p*-F substituents provide little steric hindrance to packing and also possibly reduce the driving force for metallophilic interactions through electronic effects (vide supra). The bulkier *p*-CF_3 and *p*-OMe groups in **1**/**2**, **9a**−**c**, and **10a**,**b** result in more complicated packing schemes that include CF_3···π or CH_3···π interactions, though 1.5−2.5 $\pi-\pi$ interactions per complex are still present in each case. The complexes with *ortho*-substituted aryl rings, **11**/**12**, are sterically prevented from forming any $\pi-\pi$ interactions and show only CH_3···π contacts.

The fine balance between different packing interactions is apparent in the crystallization behavior of **9**. In **9a** and **9b**, CH_3···π interactions predominate, and their combination with $\pi-\pi$ interactions and isolated Pt···Pt contacts stabilizes channels that can accommodate either CH_2Cl_2 (**9a**) or chlorobenzene (**9b**). Addition of 1,2-$C_6H_4Cl_2$ (**9c**) causes a shift to more extensive $\pi-\pi$ stacking while reducing the number of CH_3···π interactions and allowing a closer approach of the Pt atoms.

Notably, the structures of isoleptic Pt and Pd complexes are almost identical in most cases. This is true for **5a**/**6a** and **7**/**8**, which have chains of short M···M contacts, as well as for **1**/**2** and **11**/**12**, in which only longer interactions are present. Given that metallophilic interactions are expected to be stronger for Pt,[28] this suggests that these interactions do not play a dominant role in determining the solid-state structures, but instead are only one component in an array of packing forces. However, we observed[19] that the nonchain polymorph of $M(CNPh)_2Cl_2$ forms more readily for Pd (**6b**) than for Pt (**5b**), suggesting that stronger metal−metal bonding in Pt could result in different structures being obtained for the two metals in some cases. The differences observed in the structures of $M(CNC_6H_4$-*p*-$F)_2Cl_2$ (**3** versus **4**) and $M(CNC_6H_4$-*p*-$OCH_3)_2Cl_2$ (**9a**−**c** versus **10a**,**b**), although complicated, are consistent with a stronger driving force for Pt···Pt versus Pd···Pd interactions. Pd complex **4** has one less "long" Pd···Pd contact per dimer in its dimer-of-dimers structure compared with the linked dimer structure of Pt congener **3**, and the remaining interdimer M···M contact is 0.1 Å longer than those in **3**. However, **4** does not appear to achieve any greater degree of aryl $\pi-\pi$ interactions compared with **3**. Instead, the overall packing efficiency is slightly higher (68.8% for **4** versus 68.1% for **3**), allowing **4** to minimize free volume[52] and achieve more nonspecific intermolecular contacts. The differences in $M(CNC_6H_4$-*p*-$OCH_3)_2Cl_2$ structures are more complex. Compounds **9a**−**c** feature Pt···Pt contacts with staggered geometries similar to those in the chain structures **5a**/**6a** and **7**/**8**, though only **9c** has a Pt···Pt distance less than 3.4 Å, whereas **10a**,**b** contain primarily head-to-tail interactions. The degree of M···M contact in the unsolvated Pd complex **10a** is diminished relative to the solvated Pt structures **9a**−**c**, with only half the complexes in **10b** involved in a M···M contact. The comparison of the *o*-dichlorobenzene solvates is ambiguous, with fewer but shorter M···M contacts in **9c** versus **10b**. Notably, the number of $\pi-\pi$ interactions is increased for **10a**,**b** relative to **9a**−**c**, suggesting a shift in the balance of packing forces toward $\pi-\pi$ contacts, possibly at the expense of shorter M···M interactions, on moving from Pt to Pd.

Discussion of Channel Formation. The examples of **5a**/**6a** and **7**/**8** imply that a synergistic combination of aryl $\pi-\pi$ and metallophilic interactions is required to stabilize structures that feature *both* extended M···M contacts and empty or solvent-filled channels. Combinations of other interactions can also lead to channels, as shown by **9a**,**b**, but these do not contain extended metallophilic interactions. In both **5a**/**6a** and **7**/**8**, the channels are walled by isocyanide aryl rings. The square channels of **7**/**8** share a common feature with the channels of **5a**/**6a** in that each aryl *para* substituent forms an interaction with an adjacent wall of the channel (Figures 5 and 8). The CH_3 substituents in **7**/**8** expand the channels significantly relative to **5a**/**6a**. However, the larger *p*-CF_3 and *p*-OMe groups clearly cannot accommodate such an arrangement. In the case of *p*-F, the lack of a channeled structure may be due to a weaker driving force for M···M bonding (vide supra), or, alternatively, may result from an unfavorable electrostatic match between fluorine and an adjacent aryl ring. Finally, the existence of the nonchanneled polymorphs of $M(CNPh)_2Cl_2$ (**5b**/**6b**) shows that the driving force for a more efficiently packed structure[52] can outweigh the favorable combination of aryl $\pi-\pi$ and metallophilic interactions.

A survey of related compounds shows that the channels of **7** and **8** are among the largest known for structures supported by metallophilic bonding. The vapochromic compound Tl[Au-$(C_6Cl_5)_2$] was reported to have channels up to 10.47 Å wide

dx.doi.org/10.1021/ic301104a | *Inorg. Chem.* 2012, 51, 10728−10746

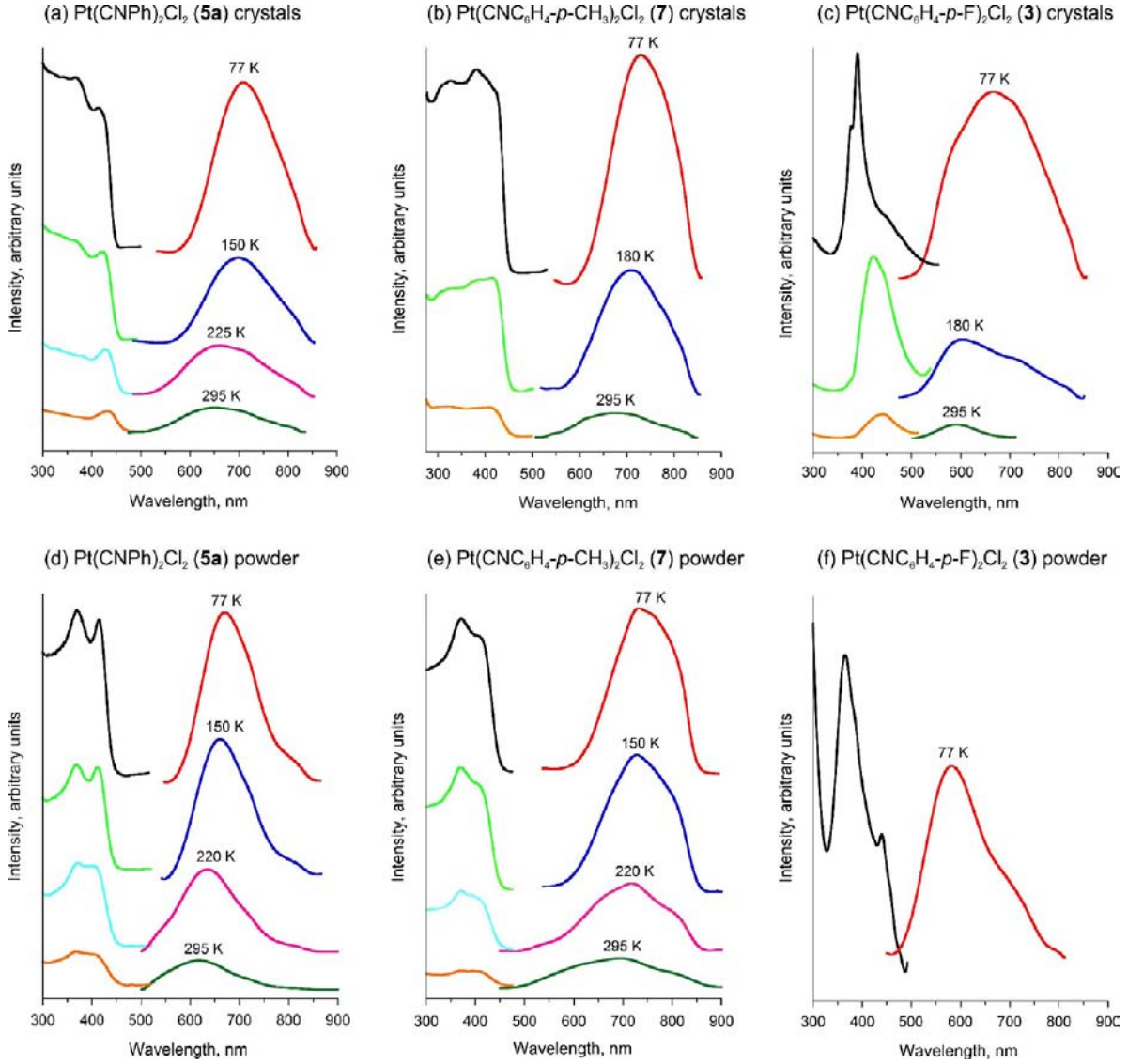

Figure 15. Luminescence spectra of macrocrystalline (a–c) and powder (d–f) samples of **5a**, **7**, and **3**. Excitation spectra were recorded at the emission maxima. Excitation wavelengths used for emission spectra are given in Table 5.

based on the distance between Au atoms.[15h] However, analysis of the structure with PLATON[42b] shows that there is no discernible void space in the unsolvated form, and solvated forms contain solvents that are bound to Tl rather occupying true channels.[15i] A gold(I) carbene complex was found to crystallize with acetone, benzene, or chlorobenzene occupying channels with maximum widths of ~5 Å.[15m] (2,2′-Bipyrimidine)$PtCl_2$ crystallizes with 2.3 Å × 7.0 Å channels that are narrower and slightly shorter than the rhombic channels of **7**/**8**,[7] yet able to accommodate N-methylpyrrolidone solvent molecules.[53] The structure of closely related $Pt(CNC_6H_4\text{-}p\text{-}C_2H_5)_2(CN)_2$ has octagonal channels with maximum widths of 4.5–4.7 Å that contain toluene or hexane,[15f] whereas $Pt(CN^iPr)_2(CN)_2$ forms channels that accommodate benzene despite their narrow widths (1.6 × 6.6 $Å^2$).[15q] A recently reported structure of (benzoquinolinate)Pt(CN^tBu)Cl has channels with widths of 2.6 × 3.9 $Å^2$ that contain $CHCl_3$.[13j] At first glance, it is surprising that the channels of **7** and **8** do not accommodate hexane or CH_2Cl_2, given that the solvent-filled channels in the above-cited structures all have smaller widths. However, closer inspection reveals that the published examples all contain deeper indentations that are wider than the maximum continuous channel widths, similarly to structures **9a**,**b**. By contrast, the channels of **7** and **8** have smooth, nonindented channel walls composed primarily of aryl ring π-surfaces, as do the narrower channels of **5a** and **6a**. Although such uniform walls could be desirable for facile diffusion of molecules into the channels, the channels of **7** and **8** do not appear to be wide enough to accommodate solvents other than H_2O despite their large continuous channel widths. The accommodation of H_2O in apparently hydrophobic, arene-walled channels in **7**/**8** is notably similar to the spontaneous uptake of H_2O by single-walled carbon nanotubes.[54]

Luminescence Studies. Luminescence in extended Pt···Pt chain structures is often attributed to excited states centered on the valence bands formed by overlap of d_{z^2} orbitals along the Pt···Pt chains.[6a,18a] Because such behavior would provide evidence for metallophilic interactions involving substantial orbital overlap, we tested large crystals (>0.7 mm) of all of the $Pt(CNAr)_2Cl_2$ complexes for luminescence.

dx.doi.org/10.1021/ic301104a | *Inorg. Chem.* 2012, 51, 10728–10746

Visible luminescence was detected for crystals of **3**, **5a**, and **7**, with each exhibiting broad, unstructured emission peaks at low energies (λ_{max} ~600−730 nm; Figure 15a−c and Table 5).

Table 5. Luminescence Data for 5a, 7, and 3

complex	excitation wavelength	T, K	λ_{max}, nm (τ, μs)
5a crystal	415 nm	295	650 (1.7)
		225	661
		150	699
		77	709 (4.1)
5a powder	415 nm	295	617 (1.1)
		220	635
		150	660
		77	670 (3.7)
7 crystals	415 nm	295	674 (1.5)
		180	709
		77	729 (5.1)
7 powder	420 nm	295	695 (0.9)
		220	717
		150	728
		77	732 (5.5)
3 crystal	390 nm	295	590
		180	603
		77	666 (5.0)
	450 nm[a]	295	591 (2.1)
		180	601
		77	619 (6.3)
3 powder	360 nm	77	582 (1.5)

[a]Emission plots for **3** at 450 nm excitation are shown in Figure S20 (Supporting Information).

Crystals of **3**, which consists of weakly linked Pt···Pt dimers, showed noticeably weaker luminescence compared with **5a** and **7**, which have uniformly short Pt···Pt distances (Table 3). None of the crystals containing isolated Pt···Pt dimers was luminescent, strongly suggesting that the luminescence of **3**, **5a**, and **7** arises from electronic states involving communication along the extended Pt···Pt chains. Luminescence spectra measured at several temperatures from 295 to 77 K showed the expected increases in intensity due to attenuation of nonradiative decay processes, as well as red shifts in the emission maxima upon cooling. Such red shifts are characteristic of luminescent Pt···Pt chain compounds and are attributed to contraction of the Pt···Pt distances at low temperature,[6a,15j,18a,S5] which strengthens metallophilic bonding and thereby raises the dσ* states of the d_{z^2} band in energy.[7] Emission lifetimes suggest phosphorescent excited states at all temperatures (Table 5).

It is well established that the emission maxima of related Pt···Pt chain structures, most notably salts of $[Pt(CN)_4]^-$, shift to lower energy as the Pt···Pt distances decrease.[5] Interestingly, the emission spectra of crystalline **3**, **5a**, and **7** do not show this trend. The emission maximum of **7** (729 nm at 77 K) is lower in energy than that of **5a** (709 nm), although the Pt···Pt distances are longer in **7**. However, compound **3** has the highest emission energy (666 nm), consistent with its longer Pt···Pt distances. Rather than correlating with Pt···Pt distances, the emission energies appear to reflect the isocyanide aryl substituent. More electron-rich arylisocyanides (e.g., *p*-Me-C_6H_4NC in **7**) shift the emission maxima to lower energies. Luminescence in Pt···Pt chain compounds has commonly been attributed either to metal-metal-to-ligand charge transfer (^{3}MMLCT) states involving dσ*(Pt)→ π*(ligand) transitions[13j,14d,15j,n,S6] or to metal-centered (^{3}MC) states involving dσ*→ pσ transitions.[5,15f,23] As the arylisocyanide ligands become more electron-rich, both the Pt dz^2($d\sigma$*) and isocyanide π* orbitals should rise in energy. The observed trend in emission maxima would be consistent with ^{3}MMLCT if these two orbitals are destabilized by different amounts, provided these differences are well reflected in the emissive excited state geometries. However, absorption spectra of dilute solutions of **3**, **5**, and **7** exhibit low-wavelength maxima that are likely attributable to d_{z^2}→ π* transitions,[S7] yet vary little as a function of ligand substituent (Figures S21−S23 and Table S4, Supporting Information). This indicates a fairly constant gap between dσ* and π* orbitals in this series, suggesting that ^{3}MMLCT-based emission maxima should also vary little, although excited-state distortions could complicate this picture.[21c,S8] We favor a metal-centered (^{3}MC) assignment for the luminescent states in **3**, **5a**, and **7**, as the Pt pσ orbitals should be little affected by ligand donor strength, whereas dσ* orbitals should be destabilized by stronger donors. This assignment is consistent with literature precedent for other luminescent Pt···Pt chain compounds containing isocyanide ligands.[15f,23]

The temperature-dependent luminescence spectra of **3** show features not observed for **5a** and **7**. Luminescence of **3** is weak at 295 K, and the emission maximum changes only slightly from 295 to 180 K before shifting to the red by >60 nm at 77 K (Figure 15c and Table 5). These observations, as well as the broadness of the 77 K emission peak and a shoulder at lower wavelength, suggest two different phosphorescent excited states that dominate at different temperatures. A blue shift in the excitation peak between 180 and 77 K is consistent with a different luminescence process at 77 K. In addition, excitation of **3** at a longer wavelength corresponding to the room temperature excitation maximum (450 nm) resulted in a 47 nm blue-shift for the 77 K emission but did not affect the emission maxima at higher temperatures (Table 5). A plausible explanation is that effective overlap of Pt $5d_{z^2}$ and 6p orbitals, which is required for luminescence based on spatially delocalized ^{3}MC states, only occurs at very low temperatures at which the weak interdimer Pt···Pt contacts of **3** are significantly contracted (vide infra). As the temperature increases, **3** behaves more as an isolated Pt···Pt dimer structure, allowing other phosphorescent states to be populated. Although ^{3}MMLCT-based emission from isolated Pt···Pt dimers is known for complexes of certain ligands,[S9] this is unlikely to account for the higher-temperature phosphorescence of **3**, given that no luminescence was observed for any of the other isocyanide-ligated Pt···Pt dimer structures (i.e., **1**, **5b**, **9a−c**). The higher-temperature emission of **3** is more plausibly attributed to an excimer-like state arising from ligand π→π* transitions in π-stacked complexes. There is precedent for excimer-based emission occurring at similar energies in Pt complexes that also show ^{3}MMLCT-based luminescence.[56b,c,60] This assignment is consistent with the greater prominence of π−π interactions in the structure of **3** compared **5a** and **7** (Table 4).

Luminescence spectra of powder samples of **3**, **5**, and **7**, which were identical to those used to grow the larger crystals, were also obtained. Powder X-ray diffraction confirmed that all three samples were composed of the same crystalline phase as the larger single crystals (Figures S24−S26, Supporting Information). The emission spectra of powdered **5** and **7**

closely resemble those of the macrocrystalline samples, with similar red shifts seen upon cooling (Figure 15d,e). By contrast, the powder sample of **3** showed no detectable luminescence at room temperature and only weak luminescence at 77 K, with the emission maximum of 582 nm matching the room-temperature spectrum of macrocrystalline **3** rather than the 77 K spectrum. We hypothesize that the delocalized ^{3}MC states responsible for the 77 K emission in macrocrystalline **3** are destabilized in smaller microcrystals, in which the Pt···Pt chains have a reduced spatial extent, allowing population of $\pi\rightarrow\pi^*$ states instead. A similar effect of crystallite size may be responsible for the blue shifts of 26−39 nm observed in the emission peak of powdered **5** relative to the macrocrystalline sample (Table 5), although this effect is not seen for **7**.

Face Indexing of Crystals. In our preliminary report,[19] face-indexing of crystals of **5a** and **6a** revealed that the preferred crystal growth axis was along the extended M···M chains. To probe whether this is a general phenomenon, we face-indexed samples of the other luminescent Pt···Pt chain compounds, **3** and **7**. Both compounds form long, rod-shaped crystals, and face-indexing confirmed that the long axis corresponds to the direction of the M···M chains in each case (Figure 16): the

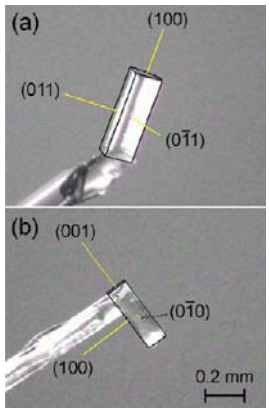

Figure 16. Face-indexed crystals of (a) **3** and (b) **7**. Yellow lines indicate face normals.

[100] lattice direction (i.e., the *a* axis) in the case of **3**, and the [001] lattice direction (i.e., the *c* axis) in the case of **7**. Complex **8**, the near-isostructural Pd analogue of **7**, also shows preferred growth along the *c* axis, corresponding to the Pd···Pd chain direction (Figure S27). Notably, the Pd 4-fluorophenyl isocyanide complex **4** forms rods similar in appearance to those of **3**, but the preferred growth axis does not correlate with any specific packing interaction. Instead, the crystals grow preferentially along the [1 $\bar{2}$ 0] lattice direction (Figure S28), which is roughly perpendicular to the direction of $\pi-\pi$ stacking and does not parallel the Pd···Pd "linked dimer" contacts. These results support the view that a combination of extended metallophilic interactions and $\pi-\pi$ stacking contributes significantly to driving force for crystal formation in **3**, **5a**/**6a**, and **7**/**8**. Complex **4** provides evidence that $\pi-\pi$ interactions alone do not provide enough thermodynamic impetus to determine the preferred crystal growth axis.

Temperature Dependence of Packing Interactions. Pt···Pt distances can shorten significantly upon cooling a crystal when extended metallophilic interactions play a prominent role in crystal packing.[15j,55] As thermal motions decrease, packing interactions that are the most favorable are expected to show the largest decreases in the relevant distances. To further evaluate the relative importance of extended M···M interactions, we have examined the temperature dependence of structures **3**, **5a**/**6a**, and **7**. For **3** and **5a**/**6a**, full structures were determined at 300 and 100−115 K, allowing direct comparisons of structural changes (Table 6). To provide

Table 6. Temperature Dependence of Selected Structural Parameters

structure	*T*	M···M (Å)	aryl $\pi-\pi$ interplanar separation	aryl $\pi-\pi$ centroid−centroid	other
5a	300 K	3.3183(8)	3.43 Å (C11−C11)	3.86 Å	CH−π 2.91 Å
			3.76 Å (C21−C21)	4.07 Å	
	100 K	3.2455(3)	3.32 Å (C11−C11)	3.82 Å	CH−π 2.90 Å
			3.56 Å (C21−C21)	3.91 Å	
6a	300 K	3.3152(3)	3.42 Å (C11−C11)	3.87 Å	CH−π 2.92 Å
			3.75 Å (C21−C21)	4.04 Å	
	100 K	3.2370(3)	3.32 Å (C11−C11)	3.83 Å	CH−π 2.91 Å
			3.56 Å (C21−C21)	3.89 Å	
3	300 K	Pt1−Pt2 3.4913(3)	3.46 Å (C11−C41 #1)	3.90 Å	
		Pt1−Pt2 [1 + *x*, *y*, *z*] 3.8809(3)	3.47 Å (C11−C41 #2)	4.15 Å	
			3.43 Å (C21−C31 #1)	3.86 Å	
			3.36 Å (C21−C31 #2)	4.26 Å	
	115 K	Pt1−Pt2 3.3747(3)	3.36 Å (C11−C41 #1)	3.72 Å	
		Pt1−Pt2 [1 + *x*, *y*, *z*] 3.7858(4)	3.41 Å (C11−C41 #2)	3.97 Å	
			3.34 Å (C21−C31 #1)	3.71 Å	
			3.31 Å (C21−C31 #2)	4.10 Å	

further insights into the temperature dependence of packing interactions, changes in the unit cell parameters of **3**, **5a**, and **7** over the 100−300 K range were also examined (Figure 17).

For **5a**, the Pt···Pt distances decrease by 2.2% on cooling from 300 to 100 K. The aryl $\pi-\pi$ interactions show an even greater decrease, with interplanar separations shrinking by 3.2% for the C11 rings and 5.3% for the C21 rings. The *c* and *b* unit cell axes of **5a** both contract by ∼2% upon cooling to 100 K (Figure 17), which can be ascribed to the shortening of the Pt···Pt distances and C21 aryl $\pi-\pi$ interactions, respectively. Interestingly, the *a* axis shows a significant lengthening (∼2%) upon cooling. This appears to be an indirect result of the decreased aryl−aryl interplanar separations. In order to accommodate closer $\pi-\pi$ interactions with neighboring complexes, the PhNC ligands bow outward slightly. This results in a larger spread between the *para* carbon atoms of the Ph groups at 100 K (C14−Pt−C24 angle 89.3° at 300 K and 91.2° at 100 K), which leads to the observed increase in *a*. Structural changes in the Pd congener **6a** are nearly identical to those seen in **5a**, with aryl $\pi-\pi$ separations again showing larger decreases than M···M distances upon cooling (Table 6).

dx.doi.org/10.1021/ic301104a | *Inorg. Chem.* 2012, 51, 10728−10746

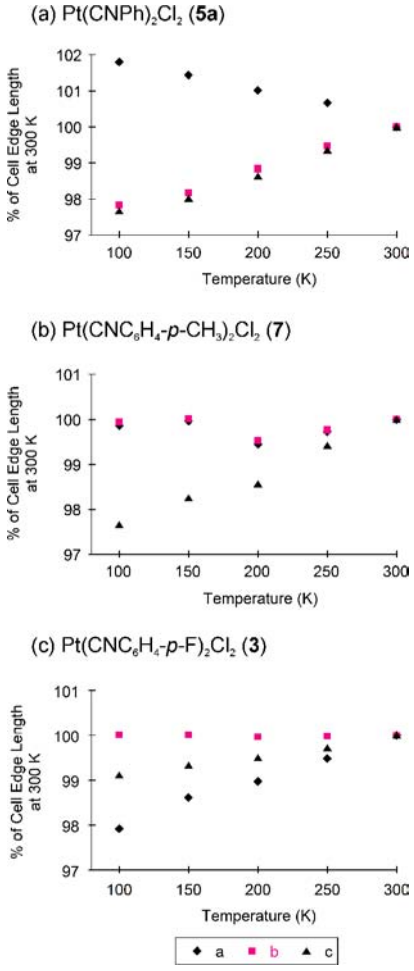

Figure 17. Temperature dependence of unit cell parameters.

The structure of the *p*-tolyl Pt complex **7** could not be determined at low temperature due to a phase change below 250 K that resulted in loss of single crystallinity. However, cell parameters were estimated over the 100−300 K range by repeatedly indexing a set of reflections that appeared to correspond to a single crystalline domain. These data indicated that the *c* axis contracted by ∼2.5%, whereas the lengths of the *a* and *b* axes stayed almost constant. The *c* axis corresponds to the direction of the extended Pt···Pt chains. The *a* axis shrank slightly relative to *b* below 250 K. We speculate that the structure of **7** is unable to accommodate contractions in both Pt···Pt distances and aryl $\pi-\pi$ stacking upon cooling, and that the structure distorts away from tetragonal symmetry by random contractions in either *a* or *b* in different regions of the crystal in order to preserve as many of these interactions as possible. This results in loss of single crystallinity at low temperatures.

The linked-dimer Pt···Pt chains of **3** show decreases in both the intradimer Pt···Pt distances (by 3.4%) and the longer interdimer Pt···Pt distances (by 2.3%). These are the largest percent contractions of Pt···Pt distances in the series. The aryl $\pi-\pi$ interactions show reductions in interplanar separations of 1.5−2.7% and decreases in centroid−centroid distances of 3.7−4.2%. The *a* unit cell axis, which corresponds to the direction of both the Pt···Pt chains and the $\pi-\pi$ stacking interactions, shows the largest change upon cooling from 300 to 115 K, shrinking by ∼2% (Figure 17). This contraction in the Pt···Pt packing axis is comparable to those seen in **5a** and **7**, despite the presence of weaker interdimer Pt···Pt contacts in **3**. We postulate that this is due to the presence of synergistic $\pi-\pi$ stacking interactions running along the same axis. Although adjacent chains of complexes are linked by aryl $\pi-\pi$ interactions along *b* (Figure 3a), this cell axis does not change measurably upon cooling. Instead, the $\pi-\pi$ stacked complexes shift diagonally as the centroid−centroid distances decrease, and this is accommodated by a slight contraction (∼1%) along *c* and a decrease of 0.8° in β.

Comparison of Bond Lengths for Pt and Pd Complexes. The crystallographic data provide an opportunity to examine differences in structural parameters for a series of isoleptic Pd and Pt isocyanide complexes. Average values of M−C, M−Cl, and C≡N bond lengths for each structure are shown in Table 7. The Pd−C bond lengths [av 1.937(1) Å] are slightly but consistently longer than the Pt−C bond lengths [av 1.911(1) Å], with an average difference of +0.027(2) Å. The M−Cl bond lengths differ by a much smaller amount in the opposite direction [av Pd−Cl 2.308(1); av Pt−Cl 2.315(1) Å; av difference −0.006(2) Å]. The differences in M−C bond lengths could plausibly be attributed to the slightly larger covalent radius of Pd [1.39(6) Å] versus Pt [1.36(5) Å],[25] but this does not explain the shorter M−Cl bond lengths for Pd. A consistent explanation is that the isocyanide ligands form stronger bonding interactions with Pt than with Pd, thereby lengthening the opposing Pt−Cl bonds via the *trans* influence. The average ν(C≡N) frequencies from the IR spectra are lower by 3−12 cm^{-1} for the Pd complexes versus the isoleptic Pt complexes in all cases except **9**/**10** (Table S3, Supporting Information), suggesting that increased π-backbonding is at least partly responsible for the observed differences in M−C

Table 7. Selected Bond Distances for Pt and Pd Complexes[a,b]

Pt structure	M−C (av), Å	M−Cl (av), Å	C≡N (av), Å	Pd structure	M−C (av), Å	M−Cl (av), Å	C≡N (av), Å
1	1.911(3)	2.312(1)	1.147(2)	**2**	1.939(2)	2.305(2)	1.147(2)
3	1.906(5)	2.316(4)	1.153(6)	**4**	1.938(3)	2.308(3)	1.141(3)
5a	1.911(8)	2.321(4)	1.15(1)	**6a**	1.939(2)	2.308(8)	1.140(3)
5b	1.910(2)	2.320(3)	1.149(2)	**6b**	1.937(2)	2.310(5)	1.144(1)
7[c]	1.918(4)	2.319(4)	1.129(4)	**8**[c]	1.936(3)	2.305(4)	1.139(7)
9a [**9**·0.5(CH_2Cl_2)]	1.913(2)	2.311(2)	1.147(2)	**10a**	1.934(6)	2.309(3)	1.144(1)
9b [**9**·0.25(PhCl)]	1.912(3)	2.311(3)	1.146(3)	**10b** [**10**·$C_6H_4Cl_2$]	1.939(4)	2.310(2)	1.148(2)
9c [**9**·0.5($C_6H_4Cl_2$)]	1.913(1)	2.315(3)	1.144(2)				
11	1.909(4)	2.319(1)	1.151(3)	**12**	1.932(1)	2.308(2)	1.145(1)

[a]A detailed listing of bond lengths and angles is given in Table S2 (Supporting Information). [b]Determined from low temperature data sets (100−115 K) unless otherwise noted. [c]Determined from data at 298 K.

dx.doi.org/10.1021/ic301104a | *Inorg. Chem.* 2012, 51, 10728−10746

bond lengths and *trans* influence. The observed shortening of C≡N bond lengths by an average of −0.004(2) Å for Pd complexes relative to the Pt analogues further supports this explanation. Structurally, the differences in metal−ligand bond lengths are minor, and they do not appear to significantly impact the crystal packing of Pt versus Pd complexes.

CONCLUSION

Metal−metal contacts of 3.5 Å or shorter are present in all studied $Pt/Pd(CNAr)_2Cl_2$ complexes except for those with ortho CH_3 groups (**11**/**12**), in which they are sterically precluded. Only in the cases of **5a**/**6a** (Ar = Ph), **7**/**8** (Ar = C_6H_4-*p*-CH_3), and **3** (Ar = C_6H_4-*p*-F) are extended chains of metallophilic interactions present. In each of these cases, $\pi-\pi$ stacking interactions between isocyanide aryl rings also feature prominently in the crystal packing network. The primary effects of aryl ring substitution are to change the steric properties of the isocyanide ligands and to create possibilities for alternative packing motifs (e.g., $CH_3\cdots\pi$ and $CF_3\cdots\pi$) that can either augment or disrupt M···M interactions, rather than to promote or to disfavor metallophilic bonding through electronic effects. However, the relative weakness of Pt···Pt bonding in *p*-F substituted **3** compared with sterically similar **5a** suggests that electronic effects may play at least a minor role in promoting metallophilic interactions. Evidence that metallophilic bonding plays an important, though probably not dominant, role in determining crystal packing arrangements is seen in the stronger M···M interactions for Pt complexes versus their nonisostructural Pd analogues in **3**/**4** and **9a**−**c**/**10a**,**b** as well as the orientation of the preferred crystal growth axes of **3**, **5a**/**6a**, and **7**/**8** along the extended M···M chains. The Pt···Pt chain-centered luminescence of **3**, **5a**, and **7**, as well as the temperature dependence of their packing interactions and cell axes, also support a substantial role for metallophilic bonding in these structures, although the latter studies also confirmed the importance of $\pi-\pi$ interactions.

This study implies that efforts to design luminescent materials based on extended metallophilic bonding cannot rely on Pt···Pt interactions to dominate molecular packing arrangements. Instead, the full array of possible intermolecular interactions must be taken into account. In particular, a synergistic combination of $\pi-\pi$ stacking and M···M contacts, with additional $CH\cdots\pi$ or $CH_3\cdots\pi$ interactions that do not disrupt these interactions, appears to be a promising formula for luminescent extended chain structures. With judicious choice of ligands, the creation of channeled, M···M chain structures with cavity sizes exceeding the 7.6 Å width obtained in the structures of **7**/**8** should be possible, creating opportunities for luminescent materials that are responsive to volatile molecules diffusing into these structural voids.

ASSOCIATED CONTENT

Supporting Information

Additional tables, packing diagrams, luminescence plots, and crystal images; UV−vis absorption spectra; powder X-ray diffraction data; and thermal ellipsoid plots. This material is available free of charge via the Internet at http://pubs.acs.org.

AUTHOR INFORMATION

Corresponding Author

*E-mail: lms@chem.okstate.edu.

Notes

The authors declare no competing financial interest.

[§]Deceased, January 2012. Most recent address: King Fahd University of Petroleum & Minerals, KFUPM Box 418, Dhahran 31261, Kingdom of Saudi Arabia.

ACKNOWLEDGMENTS

We thank the National Science Foundation (CAREER Award CHE-0645438 to L.M.S. and CHE-0911690 to M.A.O.) for funding. I.M.S. was partly supported by an REU grant from the National Science Foundation (CHE-0649162). Sri Subramanium and Yohan Mathota Arachchige (OSU) are thanked for assistance in obtaining spectroscopic data.

REFERENCES

(1) (a) Schmidbaur, H. *Gold Bull.* **2000**, *33*, 3−10. (b) Balch, A. L. *Gold Bull.* **2004**, *37*, 45−50. (c) Dias, H. V. R.; Diyabalanage, H. V. K.; Eldabaja, M. G.; Elbjeirami, O.; Rawashdeh-Omary, M. A.; Omary, M. A. *J. Am. Chem. Soc.* **2005**, *127*, 7489−7501. (d) Hayoun, R.; Zhong, D. K.; Rheingold, A. L.; Doerrer, L. H. *Inorg. Chem.* **2006**, *45*, 6120−6122. (e) Elbjeirami, O.; Omary, M. A. *J. Am. Chem. Soc.* **2007**, *129*, 11384−11393. (f) Schneider, J.; Lee, Y.-A.; Pérez, J.; Brennessel, W. W.; Flaschenreim, C.; Eisenberg, R. *Inorg. Chem.* **2008**, *47*, 957−968. (g) Doerrer, L. H. *Comments Inorg. Chem.* **2008**, *29*, 93−127. (h) Phillips, V.; Willard, K. J.; Golen, J. A.; Moore, C. J.; Rheingold, A. L.; Doerrer, L. H. *Inorg. Chem.* **2010**, *49*, 9265−9274.

(2) (a) Pyykkö, P. *Chem. Rev.* **1997**, *97*, 597−636. (b) Pyykkö, P. *Angew. Chem., Int. Ed.* **2004**, *43*, 4412−4456. (c) Pyykkö, P. *Inorg. Chim. Acta* **2005**, *358*, 4113−4130.

(3) (a) Schmidbaur, H.; Schier, A. *Chem. Soc. Rev.* **2008**, *37*, 1931−1951. (b) Katz, M. J.; Sakai, K.; Leznoff, D. B. *Chem. Soc. Rev.* **2008**, *37*, 1884−1895.

(4) Williams, J. M. *Adv. Inorg. Chem.* **1983**, *26*, 235−268.

(5) Gliemann, G.; Yersin, H. *Struct. Bonding (Berlin)* **1985**, *62*, 87−153.

(6) (a) Houlding, V. H.; Miskowski, V. M. *Coord. Chem. Rev.* **1991**, *111*, 145−152. (b) Omary, M. A.; Patterson, H. H. *Inorg. Chem.* **1998**, *37*, 1060−1066. (c) Catalano, V. J.; Malwitz, M. A. *Inorg. Chem.* **2003**, *42*, 5483−5485.

(7) Connick, W. B.; Marsh, R. E.; Schaefer, W. P.; Gray, H. B. *Inorg. Chem.* **1997**, *36*, 913−922.

(8) (a) Hunter, C. A.; Sanders, J. K. M. *J. Am. Chem. Soc.* **1990**, *112*, 5525−5534. (b) Janiak, C. *Dalton Trans.* **2000**, 3885−3896.

(9) Nishio, M.; Hirota, M.; Umezawa, Y. *The CH/π Interaction: Evidence, Nature, and Consequences*; Wiley-VCH: New York, 1998.

(10) Lindemann, S. V.; Rathore, R.; Kochi, J. K. *Inorg. Chem.* **2000**, *39*, 5707−5716.

(11) Steiner, T. *Angew. Chem., Int. Ed.* **2002**, *41*, 48−76.

(12) Metrangolo, P.; Neukirch, H.; Pilati, T.; Resnati, G. *Acc. Chem. Res.* **2005**, *38*, 386−395.

(13) (a) Vicente, J.; Chicote, M.-T.; Abrisqueta, M.-D.; Guerrero, R.; Jones, P. G. *Angew. Chem., Int. Ed. Engl.* **1997**, *36*, 1203−1205. (b) Puddephatt, R. J. *Chem. Commun.* **1998**, 1055−1062. (c) Hao, L.; Mansour, M. A.; Lachicotte, R. J.; Gysling, H. J.; Eisenberg, R. *Inorg. Chem.* **2000**, *39*, 5520−5529. (d) Hunks, W. J.; Jennings, M. C.; Puddephatt, R. J. *Inorg. Chem.* **2002**, *41*, 4590−4598. (e) Stork, J. R.; Olmstead, M. M.; Balch, A. L. *Inorg. Chem.* **2004**, *43*, 7508−7515. (f) Sundararaman, A.; Zakharov, L. N.; Rheingold, A. L.; Jäkle, F. *Chem. Commun.* **2005**, 1708−1710. (g) Zhang, J.-P.; Wang, Y.-B.; Huang, X.-C.; Lin, Y.-Y.; Chen, X.-M. *Chem.—Eur. J.* **2005**, *11*, 552−561. (h) Stork, J. R.; Olmstead, M. M.; Fettinger, J. C.; Balch, A. L. *Inorg. Chem.* **2006**, *45*, 849−857. (i) Saitoh, M.; Balch, A. L.; Yuasa, J.; Kawai, T. *Inorg. Chem.* **2010**, *49*, 7129−7134. (j) Díez, Á.; Forniés, J.; Larraz, C.; Lalinde, E.; López, J. A.; Martín, A.; Moreno, M. T.; Sicilia, V. *Inorg. Chem.* **2010**, *49*, 3239−3251. (k) Kilpin, K. J.; Gower, M. L.; Telfer, S. G.; Jameson, G. B.; Crowley, J. D. *Inorg. Chem.* **2011**, *50*, 1123−1134. (l) Yang, C.; Elbjeirami, O.; Palehepitiya Gamage, C. S.;

Dias, H. V. R.; Omary, M. A. *Chem. Commun.* **2011**, *47*, 7434−7436. (m) Lasanta, T.; Olmos, M. E.; Laguna, A.; López-de-Luzuriaga, J. M.; Naumov, P. *J. Am. Chem. Soc.* **2011**, *133*, 16358−16361.
(14) (a) Osborn, R. S.; Rogers, D. *J. Chem. Soc., Dalton Trans.* **1974**, 1002−1004. (b) Herber, R. H.; Croft, M.; Coyer, M. J.; Bilash, B.; Sahiner, A. *Inorg. Chem.* **1994**, *33*, 2422−2426. (c) Toronto, D. V.; Weissbart, B.; Tinti, D. S.; Balch, A. L. *Inorg. Chem.* **1996**, *35*, 2484−2489. (d) Yam, V. W.-W.; Wong, K. M.-C.; Zhu, N. *J. Am. Chem. Soc.* **2002**, *124*, 6506−6507. (e) White-Morris, R. L.; Olmstead, M. M.; Balch, A. L. *J. Am. Chem. Soc.* **2003**, *125*, 1033−1040. (f) Stork, J. R.; Olmstead, M. M.; Balch, A. L. *J. Am. Chem. Soc.* **2005**, *127*, 6512−6513. (g) Gussenhoven, E. M.; Olmstead, M. M.; Fettinger, J. C.; Balch, A. L. *Inorg. Chem.* **2008**, *47*, 4570−4578. (h) Nishiuchi, Y.; Takayama, A.; Suzuki, T.; Shinozaki, K. *Eur. J. Inorg. Chem.* **2011**, 1815−1823.
(15) (a) Biedermann, J.; Gliemann, G.; Klement, U.; Range, K.-J.; Zabel, M. *Inorg. Chim. Acta* **1990**, *169*, 63−70. (b) Biedermann, J.; Gliemann, G.; Klement, U.; Range, K.-J.; Zabel, M. *Inorg. Chim. Acta* **1990**, *171*, 35−40. (c) Biedermann, J.; Gliemann, G.; Klement, U.; Range, K.-J.; Zabel, M. *Inorg. Chem.* **1990**, *29*, 1884−1888. (d) Mansour, M. A.; Connick, W. B.; Lachicotte, R. J.; Gysling, H. J.; Eisenberg, R. *J. Am. Chem. Soc.* **1998**, *120*, 1329−1330. (e) Buss, C. E.; Anderson, C. E.; Pomije, M. K.; Lutz, C. M.; Britton, D.; Mann, K. R. *J. Am. Chem. Soc.* **1998**, *120*, 7783−7790. (f) Buss, C. E.; Mann, K. R. *J. Am. Chem. Soc.* **2002**, *124*, 1031−1039. (g) Kato, M.; Omura, A.; Toshikawa, A.; Kishi, S.; Sugimoto, Y. *Angew. Chem., Int. Ed.* **2002**, *41*, 3183−3185. (h) Fernández, E. J.; López-de-Luzuriaga, J. M.; Monge, M.; Olmos, M. E.; Pérez, J.; Laguna, A.; Mohamed, A. A.; Fackler, J. P., Jr. *J. Am. Chem. Soc.* **2003**, *125*, 2022−2023. (i) Fernández, E. J.; López-de-Luzuriaga, J. M.; Monge, M.; Montiel, M.; Olmos, M. E.; Pérez, J.; Laguna, A.; Mendizabal, F.; Mohamed, A. A.; Fackler, J. P., Jr. *Inorg. Chem.* **2004**, *43*, 3573−3581. (j) Wadas, T. J.; Wang, Q.-M.; Kim, Y.-J.; Flaschenreim, C.; Blanton, T. N.; Eisenberg, R. *J. Am. Chem. Soc.* **2004**, *126*, 16841−16849. (k) Wong, K. M.-C.; Zhu, N.; Yam, V. W.-W. *Chem. Commun.* **2006**, 3441−3443. (l) Gil, B.; Forniés, J.; Gómez, J.; Lalinde, E.; Martín, A.; Moreno, M. T. *Inorg. Chem.* **2006**, *45*, 7788−7798. (m) Rios, D.; Pham, D. M.; Fettinger, J. C.; Olmstead, M. M.; Balch, A. L. *Inorg. Chem.* **2008**, *47*, 3442−3451. (n) Du, P.; Schneider, J.; Brennessel, W. W.; Eisenberg, R. *Inorg. Chem.* **2008**, *47*, 69−77. (o) Ni, J.; Wu, Y.-H.; Zhang, X.; Li, B.; Zhang, L.-Y.; Chen, Z.-N. *Inorg. Chem.* **2009**, *48*, 10202−10210. (p) Ni, J.; Zhang, L.-Y.; Wen, H.-M.; Chen, Z.-N. *Chem. Commun.* **2009**, 3801−3803. (q) Drew, S. M.; Smith, L. I.; McGee, K. A.; Mann, K. R. *Chem. Mater.* **2009**, *21*, 3117−3124. (r) Ni, J.; Zhang, X.; Wu, Y.-H.; Zhang, L.-Y.; Chen, Z.-N. *Chem.—Eur. J.* **2011**, *17*, 1171−1183.
(16) (a) Exstrom, C. L.; Sowa, J. R., Jr.; Daws, C. A.; Janzen, D.; Mann, K. R. *Chem. Mater.* **1995**, *7*, 15−17. (b) Daws, C. A.; Exstrom, C. L.; Sowa, J. R., Jr.; Mann, K. R. *Chem. Mater.* **1997**, *9*, 363−368. (c) Grove, L. J.; Rennekamp, J. M.; Jude, H.; Connick, W. B. *J. Am. Chem. Soc.* **2004**, *126*, 1594−1595. (d) Grove, L. J.; Oliver, A. G.; Krause, J. A.; Connick, W. B. *Inorg. Chem.* **2008**, *47*, 1408−1410.
(17) Rawashdeh-Omary, M. A.; Rashdan, M. D.; Dharanipathi, S.; Elbjeirami, O.; Ramesh, P.; Dias, H. V. R. *Chem. Commun.* **2011**, *47*, 1160−1162.
(18) (a) Kato, M. *Bull. Chem. Soc. Jpn.* **2007**, *80*, 287−294. (b) Luquin, A.; Elosúa, C.; Vergara, E.; Estella, J.; Cerrada, E.; Bariáin, C.; Matías, I. R.; Garrido, J.; Laguna, M. *Gold Bull.* **2007**, *40*, 225−233.
(19) Sluch, I. M.; Miranda, A. J.; Slaughter, L. M. *Cryst. Growth Des.* **2009**, *9*, 1267−1270.
(20) Jovanović, B.; Manojlović-Muir, L.; Muir, K. W. *J. Chem. Soc., Dalton Trans.* **1972**, 1178−1181.
(21) (a) Schneider, W.; Angermaier, K.; Sladek, A.; Schmidbaur, H. *Z. Naturforsch., B: J. Chem. Sci.* **1996**, *51*, 790−800. (b) Aullón, G.; Alvarez, S. *Chem.—Eur. J.* **1997**, *3*, 655−664. (c) Elbjeirami, O.; Yockel, S.; Campana, C. F.; Wilson, A. K.; Omary, M. A. *Organometallics* **2007**, *26*, 2550−2560. (d) Elbjeirami, O.; Gonser, M. W. A.; Stewart, B. N.; Bruce, A. E.; Bruce, M. R. M.; Cundari, T. R.; Omary, M. A. *Dalton Trans.* **2009**, 1522−1533.
(22) Connelly, N. G.; Crossley, J. G.; Orpen, A. G.; Salter, H. *J. Chem. Soc., Chem. Commun.* **1992**, 1564−1568.
(23) Sun, Y.; Ye, K.; Zhang, H.; Zhang, J.; Zhao, L.; Li, B.; Yang, G.; Yang, B.; Wang, Y.; Lai, S.-W.; Che, C.-M. *Angew. Chem., Int. Ed.* **2006**, *45*, 5610−5613.
(24) (a) Ecken, H.; Olmstead, M. M.; Noll, B. C.; Attar, S.; Schlyer, B.; Balch, A. L. *J. Chem. Soc., Dalton Trans.* **1998**, 3715−3720. (b) White-Morris, R. L.; Olmstead, M. M.; Balch, A. L.; Elbjeirami, O.; Omary, M. A. *Inorg. Chem.* **2003**, *42*, 6741−6748. (c) Elbjeirami, O.; Omary, M. A.; Stender, M.; Balch, A. L. *Dalton Trans.* **2004**, 3173−3175.
(25) Crystallographic data indicate that Pt has a slightly smaller covalent radius than Pd. See: Cordero, B.; Gómez, V.; Platero-Prats, A. E.; Revés, M.; Echeverría, J.; Cremades, E.; Barragán, F.; Alvarez, S. *Dalton Trans.* **2008**, 2832−2838.
(26) For discussions of a similar trend in Au versus Ag, see: (a) Tripathi, U. M.; Bauer, A.; Schmidbaur, H. *J. Chem. Soc., Dalton Trans.* **1997**, 2865−2868. (b) Omary, M. A.; Rawashdeh-Omary, M. A.; Gonser, M. W. A.; Elbjeirami, O.; Grimes, T.; Cundari, T. R.; Diyabalanage, H. V. K.; Palehepitiya Gamage, C. S.; Dias, H. V. R. *Inorg. Chem.* **2005**, *44*, 8200−8210.
(27) For selected examples, see: (a) Iball, J.; MacDougall, M.; Scrimgeour, S. *Acta Crystallogr., Sect. B* **1975**, *B31*, 1672−1674. (b) Textor, M.; Oswald, H. R. *Z. Anorg. Allg. Chem.* **1974**, *407*, 244−256. (c) Canty, A. J.; Skelton, B. W.; Traill, P. R.; White, A. H. *Aust. J. Chem.* **1992**, *45*, 417−422. (d) Marino, N.; Fazen, C. H.; Blakemore, J. D.; Incarvito, C. D.; Hazari, N.; Doyle, R. P. *Inorg. Chem.* **2011**, *50*, 2507−2520.
(28) (a) Pyykkö, P. *Chem. Rev.* **1988**, *88*, 563−594. (b) Maliarik, M.; Nagle, J. K.; Ilyukhin, A.; Murashova, E.; Mink, J.; Skripkin, M.; Glaser, J.; Kovacs, M.; Horváth, A. *Inorg. Chem.* **2007**, *46*, 4642−4653.
(29) (a) Gokel, G. W.; Widera, R. P.; Weber, W. P. *Org. Synth.* **1976**, *55*, 96−99. (b) Curran, D. P.; Liu, H.; Josien, H.; Ko, S. B. *Tetrahedron* **1996**, *52*, 11385−11404.
(30) Drew, D.; Doyle, J. R. *Inorg. Synth.* **1990**, *28*, 346−349.
(31) (a) Michelin, R. A.; Facchin, G.; Uguagliati, P. *Inorg. Chem.* **1984**, *23*, 961−969. (b) Michelin, R. A.; Zanotto, L.; Braga, D.; Sabatino, P.; Angelici, R. J. *Inorg. Chem.* **1988**, *27*, 85−92.
(32) Wanniarachchi, Y. A.; Slaughter, L. M. *Chem. Commun.* **2007**, 3294−3296.
(33) *APEX2, Version 2.0*; Bruker AXS: Madison, WI, 2006.
(34) *SAINT, Version 7.23A*; Bruker AXS: Madison, WI, 2001.
(35) Sheldrick, G. M. *SADABS, Version 2.10*; Bruker AXS Inc.: Madison, WI, 2000.
(36) Sheldrick, G. M. *SHELXTL, Version 6.14*; Bruker AXS Inc.: Madison, WI, 2000.
(37) *MERCURY, Version 2.4.5*; Cambridge Crystallographic Data Center: Cambridge, U.K., 2011.
(38) Parsons, S.; Gould, R. O. *ROTAX*; University of Edinburgh: Edinburgh, U.K., 2003.
(39) Sheldrick, G. M. *CELL_NOW*; Bruker AXS: Madison, WI, 2004.
(40) Sheldrick, G. M. *TWINABS, Version 2008/2*; Bruker AXS: Madison, WI, 2008.
(41) Parsons, S. *Acta Crystallogr., Sect. D* **2003**, *D59*, 1995−2003.
(42) (a) van der Sluis, P.; Spek, A. L. *Acta Crystallogr., Sect. A* **1990**, *46*, 194−201. (b) Spek, A. L. *PLATON, A Multipurpose Crystallographic Tool*; Utrecht University: Utrecht, The Netherlands, 2007.
(43) Crystal structures of **5** (refs 19 and 20), **6** (ref 19), **11** (ref 44a), and **12** (ref 44b) have been previously reported.
(44) (a) Vicente, J.; Arcas, A.; Fernández-Hernández, J. M. *Organometallics* **2007**, *26*, 6155−6169. (b) Drouin, M.; Perreault, D.; Harvey, P. D.; Michel, A. *Acta Crystallogr., Sect. C* **1991**, *C47*, 752−754.
(45) Bondi, A. *J. Phys. Chem.* **1964**, *68*, 441−451.
(46) Aryl rings are referenced using the number of the ipso carbon.
(47) Packing indices were calculated as percent occupied volume using PLATON (ref 42b), with the van der Waals radii of both Pt and Pd set to 1.72 Å.

(48) Packing indices were calculated for low temperature structures (100−115 K) with identical van der Waals radii assumed for Pt and Pd (see ref 47).
(49) It has been proposed that methyl groups attached to phenyl rings or electronegative groups are capable of forming CH−π interactions; see ref 9, Chapter 1.
(50) de Almeida, E. T.; Mauro, A. E.; Santana, A. M.; Ananias, S. R.; Netto, A. V. G.; Ferreira, J. G.; Santos, R. H. A. *Inorg. Chem. Commun.* **2007**, *10*, 1394−1398.
(51) (a) Exner, O. In *Correlation Analysis in Chemistry*; Chapman, N. B., Shorter, J., Eds.; Plenum Press: New York, 1978, pp 439−540. (b) Shorter, J. *Pure Appl. Chem.* **1997**, *69*, 2497−2510.
(52) Brock, C. P.; Dunitz, J. D. *Chem. Mater.* **1994**, *6*, 1118−1127.
(53) Channel widths were estimated from space-filling plots of published structural data, using van der Waals radii for all atoms. Distances were calibrated from unit cell edges.
(54) (a) Pascal, T. A.; Goddard, W. A.; Jung, Y. *Proc. Natl. Acad. Sci. U.S.A.* **2011**, *108*, 11794−11798. (b) Kyakuno, H.; Matsuda, K.; Yahiro, H.; Inami, Y.; Fukuoka, T.; Miyata, Y.; Yanagi, K.; Maniwa, Y.; Kataura, H.; Saito, T.; Yumura, M.; Iijima, S. *J. Chem. Phys.* **2011**, *134*, 244501/1−244501/14.
(55) (a) Connick, W. B.; Henling, L. M.; Marsh, R. E.; Gray, H. B. *Inorg. Chem.* **1996**, *35*, 6261−6265. (b) Kato, M.; Kosuge, C.; Morii, K.; Ahn, J. S.; Kitagawa, H.; Mitani, T.; Matsushita, M.; Kato, T.; Yano, S.; Kimura, M. *Inorg. Chem.* **1999**, *38*, 1638−1641. (c) Field, J. S.; Gertenbach, J.-A.; Haines, R. J.; Ledwaba, L. P.; Mashapa, N. T.; McMillin, D. R.; Munro, O. Q.; Summerton, G. C. *Dalton Trans.* **2003**, 1176−1180.
(56) (a) Miskowski, V. M.; Houlding, V. H. *Inorg. Chem.* **1991**, *30*, 4446−4452. (b) Bailey, J. A.; Hill, M. G.; Marsh, R. E.; Miskowski, V. M.; Shaefer, W. P.; Gray, H. B. *Inorg. Chem.* **1995**, *34*, 4591−4599. (c) Lai, S.-W.; Lam, H.-W.; Lu, W.; Cheung, K.-K.; Che, C.-M. *Organometallics* **2002**, *21*, 226−234.
(57) (a) Isci, H.; Mason, W. R. *Inorg. Chem.* **1975**, *14*, 913−918. (b) Miller, J. S.; Marsh, D. G. *Inorg. Chem.* **1976**, *15*, 2293−2295.
(58) Vorontsov, I. I.; Kovalevsky, A. Y.; Chen, Y.-S.; Graber, T.; Gembicky, M.; Novozhilova, I. V.; Omary, M. A.; Coppens, P. *Phys. Rev. Lett.* **2005**, *94*, 193003.
(59) (a) Roundhill, D. M.; Gray, H. B.; Che, C.-M. *Acc. Chem. Res.* **1989**, *22*, 55−61. (b) Ma, B.; Djurovich, P. I.; Yousufuddin, M.; Bau, R.; Thompson, M. E. *J. Am. Chem. Soc.* **2005**, *127*, 28−29.
(60) Díez, A.; Forniés, J.; Fuertes, S.; Lalinde, E.; Larraz, C.; López, J. A.; Martín, A.; Moreno, M. T.; Sicilia, V. *Organometallics* **2009**, *28*, 1705−1718.